Published in final edited form as:
J Phys D Appl Phys. 2013 August 14; 46(32): 323001. doi:10.1088/0022-3727/46/32/323001.

Liquid Tunable Microlenses based on MEMS techniques

Xuefeng Zeng[1,2] and **Hongrui Jiang**[1,3,4,5,*]

[1]Department of Electrical and Computer Engineering, University of Wisconsin-Madison, WI 53706 USA

[2]Globalfoundries US Inc., 400 Stone Break Extension, Malta, NY 12020

[3]Materials Science Program, University of Wisconsin-Madison, WI 53706 USA

[4]Department of Biomedical Engineering, University of Wisconsin-Madison, WI 53706 USA

[5]McPherson Eye Research Institute, University of Wisconsin-Madison, WI 53706 USA

Abstract

The recent rapid development in microlens technology has provided many opportunities for miniaturized optical systems, and has found a wide range of applications. Of these microlenses, tunable-focus microlenses are of special interest as their focal lengths can be tuned using micro-scale actuators integrated with the lens structure. Realization of such tunable microlens generally relies on the microelectromechanical system (MEMS) technologies. Here, we review the recent progress in tunable liquid microlenses. The underlying physics relevant to these microlenses are first discussed, followed by description of three main categories of tunable microlenses involving MEMS techniques, mechanically driven, electrically driven, and those integrated within microfluidic systems.

Keywords

Microelectromechanical systems; MEMS; tunable lenses; microlenses; micro optics

1. Introduction

Miniaturizing optical system has been an active field in the past few years. The most important part in almost every optical system is its lenses. Hence, it is natural to develop millimeter- or sub-millimeter-scale lenses, called microlenses, which could be implemented in the miniaturized optical systems. Advances in technology have allowed for the design and fabrication of such microlenses with a variety of methods, such as reflow of photoresists and ultraviolet (UV) light-curable epoxies [1–6], hot intrusion by melting plastics to the lens shapes and cooling down [7], printing using inkjet printers [8], molding or embossing utilizing micromolds [3, 9]. These microlenses have already played important roles in many fields, such as imaging, especially biomedical imaging [1, 10–14], optical communication [15, 16], photolithography [2, 17], and lab on chips (LOC) [3, 18–20].

In many situations, the operation of the optical system requires varying the focal distance of the lens(es). This is commonly seen and is relative easy to realize in macro-scale optical systems by physically displacing or reconfiguring the lens combinations involved. However, such on-the-fly adjustments are often hard to realize for miniaturized systems. Therefore, there has been great interest in developing tunable-focus microlenses. For example, tunable

*To whom correspondence should be addressed. hongrui@engr.wisc.edu.

focus microlenses could tremendously benefit optical coherence tomography (OCT) and fiber endoscopy [21–25], or enable higher-performance small cameras [10, 11, 26] widely used in consumer electronics. Many methods have been investigated to develop miniature structures for tunable microlenses. These methods, in general, take advantage of the microelectromechanical system (MEMS) technologies. MEMS technologies essentially evolved and were greatly expanded from the conventional integrated circuit (IC) technologies [27–32]. Specifically, they can realize micro-scale actuators that are suitable to drive the microlenses to change their focal lengths. Depending on the driving mechanism, tunable focus microlenses can be categorized into mechanical and electrical ones. Most tunable microlenses are designed and fabricated based on traditional lenses and therefore their optical axes are perpendicular to their substrates. With the development of microfluidics, however, more tunable microlenses are utilized in microfluidic systems or LOC. In order to integrate with other components in and reduce the overall size of the system, tunable microlenses are then designed and fabricated so that their optical axes are parallel to the substrate.

In this paper, we review the progress made in the development of liquid tunable microlenses. All of these microlenses are directly made through MEMS techniques or involve some techniques developed from microfabrication. In Section 2, we first discuss about considerations of underlying physics related to the microlenses, followed by a brief description of their fabrication. As will be seen, most tunable microlenses involve liquids; therefore, we will also discuss briefly on surface tension, which is critical to the formation and tuning of the microlenses, and the effect of gravity. Mechanically- and electrically-driven tunable microlenses are discussed in Sections 3.1 and 3.2, respectively. Lab-on-a-chip (LOC) is undergoing rapid development in recent years and has numerous promising applications. Miniaturizing optical components, such as light sources, waveguides, lens detectors, and switches, and integrating them into microfluidics is a profound approach to enhancing LOC systems, especially for biological sensing, chemical analysis, microscopic imaging, and information processing [18]. Different from other microlenses, the horizontal tunable microlenses integrated in microfluidic devices have a unique character in that their optical axes are parallel to the substrates. Therefore, their mechanism, design and fabrication procedures are different and they are covered in Section 3.3.

2. General considerations of the physics and fabrication of tunable microlenses

2.1. Physics

For any optical lens, its performance is limited by physical laws and is determined by many parameters.

The first set of parameters is the aberrations, including distortion (because of the varying image magnification of the lens with respect to the distance to the optical axis), field curvature (due to the intrinsic mismatch between the curved image formed by the lens and the flat image sensor), spherical aberrations (stemming from rays of light passing different zones of the lens and thus being refracted to different focal points), coma (when the incident light rays have an angle with the optical axis of the lens), astigmatism (due to light rays away from the optical axis of the lens), and chromatic aberration (arising from the varying refractive index of the lens material as a function of the wavelength of light). Spherical aberration, coma, astigmatism and chromatic aberration reduce the sharpness of the resulting image from the lens, while distortion and field curvature degrade the image in terms of position and form. More detailed discussion of aberrations can be found in [33–35].

Even for microlenses, the dimension of the lens aperture is still on the order of millimeter or sub-millimeter, significantly larger than the wavelength of the light of interest. Therefore, geometric optics is generally still valid in describing the behavior of the microlenses, and software based on ray tracing (e.g., Zemax [36]) remain powerful tools in the design of the microlenses. However, scaling down the lens to millimeter or sub-millimeter scale does lead to other limiting factors for the microlens. Most importantly, the diffraction limit becomes much more severe as compared to large-scale lenses. The diffraction limit of a lens is ~ λ/D, where λ is the wavelength and D is the dimension of the lens aperture (e.g., diameter). The diffraction limit determines the angular resolution of the lens. Aberrations, on the other hand, carry less weight in microlenses [26]. This is a distinct difference between macro-scale lenses and microlenses.

Another important lens parameter is the f-number (F/#, or stop number, relative aperture, focal ratio), which is defined as the ratio between the focal length of the lens, f, to the diameter of the entrance pupil of the lens. The entrance pupil can be the diameter of the lens, D, itself, if no entrance pupil is implemented. When a microlens is applied for imaging, it can often be assumed that the object distance approaches infinity, or the image distance approaching f. Therefore, the spatial resolution on the imager, Δx, becomes $\lambda F/\#$. Similarly, the depth of focus, Δz, is $4\lambda(F/\#)^2$ [37]. The amount of light transmitted from an object through the lens to each unit area of the imager, Q, is inversely proportional to $(F/\#)^2$ [34]. It is thus seen that to keep the imaging performances of the microlenses on par with their macro-scale counterparts (i.e., keeping the spatial resolution, depth of focus, and relative light transmission capability unchanged), the F/# should remain comparable. For this reason, f of microlenses is also scaled down. Field of view (FOV), α, is another important parameter and can be defined as either angular FOV or linear FOV. Angular FOV is the angular range of a lens on an image sensor, while linear FOV is the ratio of lengths. Angular FOV of a lens can be calculated from the focal length of the lens, f, and the chosen dimension of the sensor, d, as $\alpha = 2\tan^{-1}(d/2f)$. If the angular FOV is less than about 10°, based on small angle approximation, linear FOV L in millimeter per meter can be calculated as

$$L \approx \frac{2\pi \cdot 1000}{360} \cdot \alpha.$$

When the microlens is used in a specific application, other limiting factors could arise. Since the light-gathering power of a lens is proportional to the area of the entrance pupil, smaller lens inevitably allows less light in. Figure 1 shows the schematic of a microlens coupled with a charge-coupled-device (CCD) imager for imaging. The image resolution will also be limited by the inter-receptor angle $\Delta\rho$ [38], defined as P/f, where P is the pitch of the CCD pixels, since two imaged points falling onto the same pixel cannot be resolved. As argued before, the image distance is approximately f. Since the pixel size of the CCD imager does not necessarily scale down with the microlens, reduced f in a microlens increases $\Delta\rho$ and deteriorates the image quality. For example, assume $F/\# = 2$, $f = 8$ mm, $D = 4$ mm, $P = 10$ μm, $\lambda = 500$ nm. $\Delta\rho$ is approximately 1.25 mrad, while the diffraction limit of the microlens itself is merely about 0.125 mrad. Assume the chosen dimension of the image sensor $d =$ 1mm, the angular FOV of the whole lens systems is 7.15° and the linear FOV is about 125 millimeter per meter.

2.2. Fabrication of microlenses

Making the microlenses takes advantage of advancements in modern microelectronic fabrications for ICs, MEMS, and microfluidics that can realize large scale, low cost, and precise manufacturing. Similar to microelectronic and MEMS devices, the fabrication process of microlenses starts with a certain substrate, and involves building up the device structure using different materials. The substrate materials utilized range from silicon and other semiconductor materials to glass and polymers. The materials involved in forming the

microlense structure cover a wide range, including semiconductors, dielectric inorganic materials, metals and polymers. The lens materials are often liquids or combination of liquids and solids. In this article, we focus on microlenses whose materials are transparent in visible light wavelength. The actual fabrication of the microlenses could involve many steps and utilize many techniques developed for IC, MEMS and microfluidics in the past decades. Basic fabrication steps include thin film deposition, photolithography, and etching. Other techniques are also widely used, such as lift-off process, annealing, liquid-phase photopolymerization, micromolding, soft lithography, electroplating, sacrificial process, bonding, surface modification, and laser-assisted process. To make tunable microlenses, it is critical to provide micro-scale actuators, which is one of the focuses of MEMS technologies. Hence, MEMS plays an especially important role in the tunable microlens technologies. Owing to limited space, we will not go into depth in the discussion and description of various IC, MEMS and microfluidics fabrication techniques. More details on this topic can be found in a few excellent references [27–32, 39–44].

2.3. Liquid microlens, surface tension and effect of gravity

As will be seen later, many types of tunable microlenses are based on liquid droplets or curved interfaces involving liquids. The change in the radius of curvature of such a droplet or interface results in the change in the focal length of the resultant microlens. Surface tension thus plays a critical role in the formation and operation of these tunable microlenses, as it has strong influence on the shape of the droplets and interfaces.

An important concept related to surface tension is the contact angle, the angle at which a liquid and vapor interface at a solid surface. Figure 2 shows the measured contact angles of a water droplet on a native polydimethylsiloxane (PDMS) surface, a PDMS surface coated with octadecyltrichlorosilane (OTS), and a PDMS surface treated with oxygen plasma, respectively. As can be seen, the contact angle depends on the solid surface properties, which in turn could be adjusted. The contact angle can be found referring to Figure 3, which shows the boundary of a liquid droplet on a solid surface. The surface tensions between each pair of phases – liquid (*l*) vapor (*v*), and solid (*s*) – are denoted as s. Setting the droplet at equilibrium at the boundary leads to zero net force, which yields:

$$\cos\theta=(\sigma_{sv}-\sigma_{sl})/\sigma_{lv} \quad (1)$$

which is the well-known Young equation. This equation implies that the contact angle (called static contact angle) would be constant, as the surface tensions are constants only dependent on the materials involved. This is a common misconception and in fact is counterintuitive, as a water droplet tending to move forward along a solid surface should have a larger contact angle at the front (called advancing contact angle) and a smaller contact angle at the back (called receding contact angle) [45, 46]. When deriving the contact angle in Eqn. (1), we should have included other external forces exerted onto the droplet, such as gravity and pressure. The existence of advancing and receding contact angles, or contact angle hysteresis [45, 46], is the underlying tuning mechanism of many tunable liquid microlenses. For example, Figure 4 shows a tube whose top half of the inner surface is hydrophobic and the bottom half hydrophilic. When water is filled up to the hydrophobic-hydrophilic boundary, a water meniscus is pinned. If gravity is ignored, adjusting the pressure difference across the meniscus between air and water would change the contact angle in a certain range. Because of the differences in the refractive indices of water and air, the resultant water to air interface presents a liquid lens with tunable focal length.

In the discussion of Figure 4, we neglected gravity. In reality, gravity will affect the shape of the liquid lenses. However, as the lens is scaled down to millimeter to sub-millimeter scale, the surface tension becomes a much more dominant force compared to gravity. Figure 5

demonstrates the effect of gravity on cylindrical lenses formed at junctions in microfluidic channels [47]. When a water droplet in a microchannel with a rectangular cross-section is pressurized to protrude out of a T-shaped-junction, a cylindrical water meniscus is formed owing to surface tension; adjusting the pressure across the resultant cylindrical lens varies the radius of curvature, as shown in Figure 5(a). The model was simplified in Surface Evolver to determine the shape of a free surface by the principle of minimum energy, considering the effect of gravity and other boundary conditions and constraints. The surfaces of the droplet inside the channel [confined in the framework of the solid red lines in Figure 5(b)] were set to be stationary in all three dimensions, while the displacement degrees of freedom of the surface of the lens protruding out of the junction (depicted by the framework of the spotted red lines) were not confined. The contact angle between the liquid and the inner channel surface was set to be 90°. The free surface evolved from a cuboid to the ultimate surface with the minimal free energy. Gravity effect can be neglected when the height of the lens droplet is low, 0.5 mm in Figure 5(b). When the droplet height increases, as shown in Figure 5(c) and (d), under the gravity effect, the shape of the free surface is distorted and cannot be considered as perpendicular to the substrate, which affects the optical property of the liquid lens. In general, if the scale of the liquid microlens reaches millimeter or sub-millimeter, or □L or sub- □L in volume of the droplets, the effect of gravity becomes much less [47–49].

3. Tunable microlenses

Microlenses can be categorized as fixed or tunable, where the difference lies in whether the focal length of the microlens can be varied. In many optical systems, combinations of multiple lenses are often used. In these cases, although each individual lens can be fixed in its focal length, it is possible to change the overall focal length of the complete lens combination through displacement and reconfiguration of the lenses. This approach is also taken in micro-optical systems where fixed focus microlenses are implemented and driven by micro-scale actuators for displacement or reconfiguration [50]. However, in the following discussion, we will focus on those microlenses whose focal lengths are individually tunable.

3.1. Mechanically driven tunable microlenses

Most of mechanically tunable microlenses are formed by a circular chamber covered with a thin flexible membrane. The membrane deforms when the pressure in the chamber changes through external actuation. In addition, some microlenses are formed through air-liquid or liquid-liquid interfaces (immiscible and with different refractive indices), and these interfaces can also be varied by applying pressure. Then radii of curvature of the spherical membranes, in the former type, or interfaces, in the latter type, are adjusted and the focal lengths of the resultant microlenses are tuned.

3.1.1. Tunable microlenses through pneumatic pressure—The initial design of tunable microlenses in a chamber covered with a thin membrane was inspired by crystalline lenses of human eyes. Ahn *et al.* reported a variable focusing lens with a thin glass diagram [51]. The glass diagram was 1 cm × 1 cm square and the thickness was 40 □m. Due to the relatively high Young's modulus of the glass diaphragm, a large pressure was needed to deflect the membrane. In addition, when the deflection did occur, the membrane was quite sensitive to any change in pressure. In order to achieve larger deformation of the membranes and the resulting curved surfaces, soft materials such as polymers were therefore used to replace hard glass.

A fluidic adaptive lens consisting of a fluidic chamber covered with a thin PDMS membrane was reported [19, 52, 53]. Figure 6 shows the cross section of such a microlens tuned through pneumatic pressure. The chamber between the bottom aperture substrate and the

PDMS membrane was filled with a working fluid. Different working fluids, including water and oil, were used for refractive index matching. The fluid was pumped into or out of the chamber through the microchannel utilizing an external micropump. During this process the fluid pressure varied and changed the curvature of the lens, causing a shift in the focal plane. The shape of the membrane and thus the optical power of the lenses were changed. In Figure 6, both plano-convex and plano-concave lenses were accomplished.

Besides the planar bottom surfaces, pre-defined concave [54], convex [55], and bi-convex [56] surfaces could be utilized along with polymer membranes to provide high numerical aperture for the produced microlenses. By employing two free polymer membranes, tunable microlenses covered with polymer membranes on both top and bottom were designed for large field of view (FOV) and numerical aperture values [57, 58]. Besides single-focus microlenses, Yu *et al.* presented an intriguing design based on the standard fluid-filled microlens with bi-focal capability. The polymer membrane had different thickness in the inner region and in the peripheral region. The focal length in the central region could be gradually adjusted from 46 mm to 10 mm when the pressure was changed from 200 Pa to 9.5 kPa, whereas the tunable range was from 57 mm to 15 mm in the peripheral region [59].

Different from other microlenses with water or oil as the working fluid, Xiong *et al.* used an aqueous solution of 2.5% poly-N-isopropylacrylamide (PNIPAAm) for the lens fluid [60]. PNIPAAm is a thermosensitive polymer whose polymeric chains exhibit changes around its lower critical solution temperature (LCST). At temperatures below the LCST, the intermolecular hydrogen bonds between the amide group of the PNIPAAm chain and the water molecules are predominant. The polymer chains then expand in water, resulting in a transparent liquid. When the temperature rises above the LCST, the PNIPAAm chains collapse and form clusters of polymer chain coils. The coiling of the polymer chains strongly scatters the incident light, reducing the transmittance through the fluid [60]. Similar to other lenses, the microlens was tuned by controlling the pressure in the chamber. In addition, light transmission of the microlens was also controllable. The focal length and the transmittance were controlled by the volume of liquid and temperature separately and independently [60].

In order to compare the existing pneumatically-driven tunable microlenses discussed above, we have summarized some important parameters in Table 1 for reference [61].

3.1.2. Liquid tunable microlenses actuated by stimuli-responsive hydrogels—

Pneumatically changing the pressure in the chambers is one of the main methods used in most systems. There are, however, other methods to change the shape of the membranes and thus varying the focal length of microlenses. Ren *et al.* presented a design to vary the focal length by changing the aperture size of a microlens [62, 63]. They used a lever actuator to control the movement of rotatable impellers, which in turn imparted a pressure to the fluid-filled lens. The focal length of microlenses could also be changed by re-distributing the liquid in the chamber through pressure [64]. Of these methods, microlenses tuned through stimuli-responsive hydrogels have attracted much attention.

3.1.2.1. Microlenses actuated through thermo- or pH-responsive hydrogels: Jiang's group used stimuli-responsive hydrogels to sense the change in temperature [65, 66] or pH [65, 67] in the surroundings of liquid microlenses and to control their shapes accordingly. The actuation of the hydrogels is reversible and depends on change in the environmental stimuli.

Microlenses can be formed through a meniscus between immiscible liquids, such as water and oil. Dong *et al.* used this meniscus between water and oil as an optical lens and adjusted

its focal length by changing the curvature of the meniscus [65]. Figure 7 shows the design and mechanism of the microlens. The microlens consisted of a stimuli-responsive hydrogel ring placed within a microfluidic channel system, and sandwiched between a glass plate and an aperture slip. The aperture slip had an opening centered over the ring. The microchannels were filled with water, and oil was placed on top of this structure and capped with a glass cover slip. The sidewall and bottom surface of the aperture were chemically treated hydrophilic and the top surface hydrophobic to pin the water–oil meniscus along a hydrophobic–hydrophilic (H–H) boundary, which was the top edge of the aperture opening. When exposed to an appropriate stimulus, the hydrogel ring underneath responded by expanding or shrinking, owing to the absorption or release of water via the hydrogel network interstitials [68]. This led to a change in the volume of the water droplet located in the middle of the ring. The net volumetric changes resulted in a change in the pressure difference P across the water–oil interface, which in turn would determine the geometry of the liquid meniscus. Because the meniscus was pinned at the H–H boundary and kept stationary, volume changes were translated into a change in the curvature of the meniscus, and hence the tuning of the focal length of the microlens. The authors demonstrated microlenses responsive to temperature and pH values, using respective responsive hydrogels: a thermo-responsive hydrogel based on *N*-isopropylacrylamide (NIPAAm), and two pH-responsive hydrogels based on acrylic acid (AA) and 2-hydroxyethyl methacrylate (HEMA), and 2-(dimethylamino)ethyl methacrylate (DMAEMA) and HEMA, respectively [65, 66].

Figure 8(a) shows how a temperature-responsive microlens adjusted its focal length in both positive and negative regimes as the temperature was varied. A response time of 20–25 s was observed for the device [65].

Figure 8(b) shows the focal length variation of a pH-responsive liquid microlens with respect to the pH value of its aqueous environment [65]. The response time of the pH-sensitive microlens was approximately 12 s.

Besides using an enclosed elastic polymer ring made of stimuli-responsive hydrogel for the actuators, Dong *et al.* further implemented hydrogel-actuated liquid microlenses by harnessing the expansion and contraction of the hydrogel microstructures in all three directions to tune liquid microlenses in microfluidic channels [67].

Figure 9 shows the mechanism of this type of hydrogel-driven liquid microlens [67]. A set of microposts made of pH-responsive hydrogel was photopatterned in a microfluidic chamber. A circular aperture was formed in a flexible polymer slip. The sidewall and top side of the aperture were treated hydrophilic and hydrophobic, respectively, similar to the previous case. Again, since aqueous solutions remained only on hydrophilic pathways at pressures below a critical value, part of the water-based liquid attached to the sidewall could form a liquid meniscus dropping downward at low pressures and protruding upward at high pressures. The water-based liquid containing stimuli acted as the lens liquid, flowing in the chamber; oil was used to prevent the evaporation and also served as the lens liquid. The pinned water-oil interface again formed the liquid microlens. When the environmental pH changed, the hydrogel micro-posts could expand to bend the flexible aperture slip up or restore to its original position at the contracted state. Correspondingly, the liquid meniscus could bow downward or be pressed to bulge out of the aperture. The shape of the microlens was changed in terms of the angle to the aperture slip; therefore the focal length of the microlens was tuned.

The hydrogel-driven tunable liquid microlenses can be extended to microlens arrays in which microlenses can be individually and independently tuned in focal length. Zeng *et al.*

demonstrated the feasibility of this concept, as shown in Figure 10 [69]. Figure 10(a) shows the optical image of one 5×6 microlens array before filling the lens liquids. The image was taken by a camera from an oblique angle. Each microlens in the array could be actuated individually by controlling the temperature locally. Resistive microheaters were placed under the microlens array and each microheater was connected to an individual temperature controller. Due to the individual tuning in focal length, the microlenses in the array could image objects independently.

3.1.2.2. Microlenses actuated through nanoparticles-embedded hydrogels: Zeng *et al.* extended the hydrogel-driven liquid microlens technology and presented a liquid variable-focus microlens tuned by light utilizing light-responsive hydrogels [70]. Figure 11 shows the schematics and optical images of a tunable liquid microlens actuated by infrared (IR) light-responsive hydrogel at its diverging and converging states, respectively. The device had the same mechanism as the previous devices in Section 3.1.2.1 but used different, modified hydrogel. Multiple microposts made of IR light-responsive hydrogel were defined in a water container to actuate the microlens under IR light irradiation. The IR-light-responsive hydrogel consisted of a thermoresponsive NIPAAm hydrogel and water-soluble gold nanoparticles with distinct and strong optical absorption at the IR spectrum, which has high heat efficiency. With the IR light source was turned on, the gold nanoparticles absorbed the IR light, generating heat to cause the hydrogel to contract. When the IR light was turned off, the heat dissipated to the surrounding fluid and the hydrogel expanded back to its original volume. Such volumetric change could thus change the radius of curvature of a pinned water-oil interface, as in previous devices. Hence, the tuning of the focal length of the liquid microlens formed via the water-oil interface was controlled by the IR light [70].

One important application of such tunable microlenses is for endoscopes [25]. In recent years, due to technical improvements, such as the invention of wireless capsule endoscopy [71] and robotic surgery [72], minimally invasive surgery aided with endoscopes has become a common medical procedure. Current fiber endoscopes use single optical lenses, such as rod lenses and gradient index (GRIN) lenses, at the distal ends of fibers or in front of CCD sensors for imaging [73]. However, the focal length of these single lenses is not tunable and it is difficult to manufacture and assemble a conventional zoom lens in an endoscope due to its small space inside. Hence endoscopic surgeons need extensive training owing to the need for constant and skillful manual maneuvering of the endoscopes during procedures [74].

Tunable-focus microlenses integrated at the end of fiber endoscopes could scan the areas of interest with minimal or no back-and-forth movements of the scopes themselves. Benefitting from variable focal length of the microlenses, different depth of focus and thus spatial depth perception can be obtained in the serial images acquired. Based on their accomplishment on liquid microlenses actuated through IR-light-responsive hydrogel described in the prior section, Zeng *et al.* demonstrated prototype endoscopes with tunable-focus liquid microlenses integrated at their distal ends and actuated through IR light [25, 75].

Figure 12 shows the schematics of such a prototype endoscope [25]. Two sets of optical fibers – one for actuation and one for image acquisition - were connected to the back side of the microlens. IR light was transmitted via the actuation optical fibers to stimulate the hydrogel microstructures and thus vary the focal length of the microlens at the end of the fibers. Images from the tunable-focus microlens were transferred to a camera via the image acquisition fiber bundle.

Such endoscopes were demonstrated to be able to obtain clinically relevant images [25]. An endoscopic environment was constructed to simulate the human colon and was observed by

the endoscope. Simulated tissue was used to represent colonic polyps with diameters ranging from 3 mm to 10 mm, mimicking the real polyps [76]. Figure 13 shows the frame sequence of the focused images of the simulated colon and polyps obtained from an endoscope in one scanning cycle.

3.1.2.3. Microlens arrays on flexible and curved surfaces: Zhu, *et al.* later realized responsive-hydrogel-driven microlenses arranged on non-planar surfaces [77, 78], in which tunable liquid microlenses were fabricated onto flexible polymer substrates and wrapped onto a dome-like structure. This work was inspired by the compound eyes of insects that are ominipresent in nature. A compound eye consists of many small eyes called ommatidia, generally small, individual lenses. These ommatidia are arranged on a spherical structure; a conspicuous advantage of this design is the large FOV. On the other hand, these ommatidia are not tunable in their focal length, thus having lower resolution [38]. The work by Zhu *et al.* is intriguing in that it combines the benefits of tunable liquid microlenses and the large FOV offered by compound eyes. Figure 14 is a photo of a tunable liquid microlens array with six elements fabricated on a hemisphere [78]. The microlenses were made in individual islands that were connected via thin polymer bridges. Therefore, the stress caused by the wrapping of the whole structure onto the non-planar surface mostly appeared in the bridge structures rather than in the islands. This was critical to ensure that the microlenses would not experience much stress and distortion which would otherwise severely affect their optical performance.

3.2. Electrically driven tunable microlenses

The earliest tunable focus microlenses were made of nematic liquid crystals (LCs) in 1979 [79]. Later various structures and LC materials were utilized for tunable focus microlenses [80–89]. The LC molecules are homogeneously aligned to the substrates with a small pre-tilt angle. When a relatively low voltage is applied, the LC molecules are forced to tilt according to the pre-tilt direction. Since the LC is birefringent, meaning that the refractive index depends on the applied voltage and the propagation direction of light, the orientation of the molecules would lead to various focal lengths of the microlenses. In this paper we will only cover the tunable focus microlenses with movable parts. More details about the LC-based tunable focus microlenses can be found in [61, 90].

3.2.1. Liquid microlenses encapsulated with a polymer thin film driven by electrostatic forces—

Binh-Khiem *et al.* presented a method to change the volume of encapsulated liquid by using an electrostatic force [91]. A parylene film was chemically deposited onto nonvolatile liquids under low-pressure conditions. The liquid surface was covered with a flexible thin polymer film and the liquid droplets possessed both shape and surface flexibility. Furthermore, the deposited parylene film was smooth and transparent enough for optical use. The shape of the encapsulated liquid droplets could be altered by electrostatic interactions.

Figure 15(a) shows the structure of such a liquid lens packaged in a parylene thin film [91]. The lens liquid was encapsulated in a parylene film. A thin gold layer deposited on the parylene film served as the upper electrode. The liquid microlenses were fabricated on a glass wafer sputtered with a patterned conductive indium-tin-oxide (ITO) layer. Liquid droplets were deposited onto the substrate surface. After depositing parylene onto the droplet surface, the upper gold electrode was deposited on the parylene film. The total transmittance of the lenses was about 62% at the wavelength of 650 nm [91].

When a voltage was applied, the electrostatic force would pull the two electrodes toward each other. As shown in Figure 15(b), the pulling force was mainly induced around its

circular perimeter because of the short distance from the dome to the lower electrode, thus stronger force. The upper electrode was attracted towards the lower electrode from this perimeter. Since the liquid volume inside was kept constant, any deformation from the initial spherical shape resulted in the expansion of the parylene film and an increased total surface area. As a result, the height of the droplet increased while the radius of its circular base decreased until the electrostatic force balanced the elastic force from the deformed parylene film. Such deformation also caused the lens surface curvature to increase, which in turn decreased the focal length. The lens surface remained spherical throughout the deformation. When the applied voltage was removed, the droplet returned to its initial shape due to the elasticity of the parylene film [91].

A decrease in focal length to 20% of its initial value (3.7 mm) was measured when 150 V was applied to a liquid lens of 1 mm in diameter and 60 μm in height. The 5-mm-diameter lenses could be switched by a rectangular voltage of 5 Hz with a delay of less than 0.03 s; smaller lenses could be switched by voltages of higher frequencies. The lens actuation showed a good repeatability with a stable hysteresis [91].

3.2.2. Tunable-focus liquid microlenses using dielectrophoretic effect—Cheng *et al.* introduced a packaged liquid lens which was actuated by dielectric force [92]. Figure 16(a) depicts the configuration of sucha liquid lens actuated by dielectric force. The liquid lens consisted of a 15 μL liquid droplet with a lower dielectric constant and a sealing liquid with a higher dielectric constant. The bottom diameter of the droplet was 7mm when no voltage was applied. The two liquids were injected inside a 3mm-thick polymethyl methacrylate (PMMA) chamber formed and sealed between two ITO glass substrates. The concentric ITO electrodes on the bottom glass substrate were coated with 1 μm-thick Teflon to reduce friction between the droplet and the glass substrate. The width and spacing of the ITO electrodes were both 50 μm. The mass density of the sealing liquid was adjusted to match that of the droplet in order to minimize the gravitational effect, because the gravitational effect may induce nonuniform deformation of the droplet profile, causing optical aberrations. When a voltage was applied across the electrodes, a dielectric force was exerted onto the droplet due to the difference in the dielectric constants of the two liquids. The dielectric force shrank the droplet, increasing the contact angle of the droplet on the glass surface and shortening the focal length of the liquid lens. Figure 16(b) shows the images of an object (a word “Green”) captured using the liquid lens at the rest state and at 75 V, respectively. At the rest state, the liquid lens had a long focal length due to the smaller, intrinsic contact angle of the droplet. At 75 V, the shortened focal length rendered a magnified virtual image. Similar mechanism has been utilized to form liquid microlens arrays by Ren *et al.*. When the voltage increased from zero to 200 V, the focal length of the liquid lens varied from 34mm to 12mm [93].

3.2.3. Tunable-focus liquid microlenses using electrowetting—Electrowetting has become one of the most widely used tools for manipulating liquids by surface tensions. This is the concept that has also become known as electrowetting on dielectric (EWOD) [49]. In electrowetting, one generically deals with droplets of partially wetting liquids on planar solid substrates, as shown in Figure 17 [49]. In most applications of interest, the droplets are aqueous salt solutions with a typical size on the order of 1 mm or less. The ambient medium can be either air or another immiscible liquid; oil is often utilized. Under these conditions, the Bond number $B_0 = \sqrt{g\Delta\rho R^2/\sigma_{lv}}$. Here g is gravitational acceleration, $\Delta\rho$ is difference in density of the two phases, R is characteristic length and γ_v is surface tension of the interface. The Bond number measures the strength of gravity with respect to surface tension, smaller than unity. Therefore we could neglect gravity in most cases.

In the absence of external electric fields, the behavior of the droplets is determined by surface tension alone. When a voltage is applied onto an electrolyte droplet on an electrode surface, the contact angle between the droplet and the surface follows the applied voltage.

$$\cos\theta = \cos\theta_Y + \frac{\varepsilon_0 \varepsilon_1}{2 d \sigma_{lv}} (V - V_0) \quad (2)$$

where θ_Y and θ are the contact angle before and after applying the voltage, ε_0 and ε_1 are dielectric constant of the thin film, d is the thickness of the film, and V and V_0 are the initial voltage and the applied voltage, respectively [49, 94].

One of the first proofs of concept of liquid lenses utilizing electrowetting was reported by Gorman *et al.* [95]. A hexadecanethiol (HDT) drop spread on a gold surface held at 0 V underwater and formed a hydrophobic monolayer under the drop. When the drop was on the surface at −1.7 V, it focused light through it. Electrowetting-based liquid lenses have since been further developed after the landmark work by Gorman *et al.* Berge *et al.* reported an optical lens using a water droplet [96]. Figure 18 is a schematic representation showing the principle of the operation of such a liquid lens. A cell contains two immiscible liquids, one being insulating and non-polar, the other being a conductive water solution. The liquids are transparent with different refractive indices, but with the same density. This ensures that gravity does not deform the liquid-liquid interface, which remains spherical independent of the orientation of the cell. The insulating liquid bears the shape of a drop in contact with a thin insulting window. The surface of the window is hydrophobic, so that naturally the insulating liquid would dwell on it. A transparent electrode is deposited on the external side of the window, called the counter-electrode. Application of a voltage between the counter-electrode and the conducting liquid favors the wettability of the surface by this same liquid, deforms the interface, and thus changes the focal length. The applied voltages are usually quite high for electrowetting-based lenses. Nonetheless, the actual electrical power consumption is very small because since power is only consumed during the switching and tuning of the lens.

Krupenkin *et al.* reported a planar electrode system for electrowetting based liquid lens [97]. In their work, they did not impregnate the substrate surface with any lubricant. Instead, they attempted to separate the droplet from the substrate surface by creating conditions under which a “lubricating” liquid would penetrate spontaneously under the droplet. This lubricating liquid should be immiscible with the primary liquid that would form the droplet. A thin layer of such a “lubricant” would prevent the droplet from directly interacting with the contaminants and inhomogeneities of the solid surface, thus completely eliminating the contact angle hysteresis and the stick–slip behavior [98]. By utilizing the split electrodes, Yang *et al.* used the electrowetting to precisely align the liquid microlens on the substrate. The liquid microlens was exposed to UV light to initiate polymerization and thus lock in its position and shape. The solidified microlens was then thermally and mechanically robust and able to retain indefinitely its shape, size and position, without any applied voltage [99].

To overcome the issue of evaporation, Kuiper *et al.* demonstrated a liquid lens consisting of two immiscible liquids inside a chamber for miniature cameras [11]. Figure 19 (a) and (b) show the schematic cross section of the variable lens without and with voltage, respectively. Figure 19 (c) and (d) show the schematic cross section of the module and photographs of the entire camera with the electrowetting-based lens. The height of the lens stack was 5.5 mm measured from the image sensor. The lens had an F/# of f/2.5 and a field of view of 60°. A commercial image sensor (Philips OM6802), having 640×480 pixels with a size of 5.0×5.0 μm^2 was used. The entrance pupil diameter was 1.43 mm and the focal length was adjustable between 2.85 mm for objects at 2 cm and 3.55 mm for objects at infinity. The

electrowetting cell was set between two plastic injection-molded lenses. A flat glass plate closed the cylinder on the oil side, whereas a truncated glass sphere mounted on a thin metal diaphragm closed the side of the salt solution. The outer diameter of the cylinder was 4 mm, the inner diameter 3 mm, and the height 2.2 mm. The flexible metal diaphragm compensated partially the mismatch in the thermal expansion between the liquids and the cylinder. The achromatized lens stack had a high optical quality. The camera was able to focus faster than the refresh rate of the imager [11].

3.2.4. Electrowetting based microlens on a flexible curvilinear surface—The electrowetting-based lenses discussed so far are made on flat and mostly rigid substrates. Li *et al.* have extended the technology to fabricate electrowetting-based tunable liquid microlens on flexible polymer surfaces [100]. Figure 20(a) shows the schematic of such as lens. The lens structure was first formed as a polymer island housing the lens on a thin polymer substrate. Both the housing island and the substrate could be made of PDMS, although other polymers could also be used. The whole structure could then be wrapped conformally onto a curvilinear surface. Figure 20(b) shows such a lens made onto a commercial contact lens. The peculiar attribute of flexibility imposes stricter requirements on the fabrication processes, though, compared to those on flat, rigid substrates [100].

3.2.5. Electrochemically activated adaptive liquid microlens—Lopez *et al.* devised a surface-tension-bounded liquid lens with a pinned contact line that was activated using electrochemistry [101]. The lens was formed by the free surfaces of a liquid overfilling a circular hole of radius R, as shown in Figure 21. The contact circles of the liquid were pinned by using a non-wetting material, which also aligned the optical axis with the center of the orifice. Surface tension was made to change on one capillary surface relative to the other by utilizing a redox surfactant solution as the lens medium [101].

Activation of the liquid lens was achieved using a water soluble ferrocenyl surfactant, whose surface activity could be controlled electrochemically [102]. Application of a voltage difference across the lens then produced a reversible reduction-oxidation process that modified the surface activity of that surfactant. The surface tension increased where oxidation occurred and decreased where reduction occurred with a magnitude of approximately 8 dyn/cm. The total change in surface tension (16 dyn/cm) was more than 1/5 of the surface tension of pure water. This difference in surface-tension modified the response of the system, resulting in a redistribution of the liquid. The orientation of the anode and the cathode (top versus bottom electrode) determined the amount of change in the focal length. In the case where the voltage applied and the corresponding changes in surface tension had the net effect of equalizing V_{top} and V_{bottom}, there would be a large volume displacement but little focal length change since r_t, r_b, and d would not change significantly. On the other hand, if the applied voltage and the resultant changes in surface tensions drove either V_{top} or V_{bottom} towards zero, the focal length increased by a factor of about 3 for the air/water system [101].

3.3. Horizontal microlenses integrated within microfluidics

Besides the observation and light activation from the top, there are a lot of requirements for light control and manipulation from the sides of microfluidic channels. Some researchers have dealt with the fabrication of embedded waveguides using various materials and technologies [1, 103–108]. One key question is how to guide light into the waveguides. Multiple designs have been proposed with optical fibers integrated into the microchips [1, 105, 109]. The key components in these designs are in-plane microlenses, and the system is called optofluidics. It benefits from the small scale of microfluidics and utilizes single or multiple fluidic flows to manipulate, guide or control light in micro- or even nano- scale.

Many investigators have demonstrated microlenses based on the optofluidic approach. The optical axes of these microlenses are parallel to the substrate of microlenses, distinctly different from what we have seen in prior sections.

3.3.1. Tunable and movable liquid microlenses—Dong *et al.* presented a tunable and movable liquid microlens *in situ* fabricated through a relatively simple process by pneumatically manipulating fluids within a microfluidic network [18]. A de-ionized (DI) water droplet segmented by air was guided to a T-shaped junction in a microchannel by pneumatic fluid manipulation. After chemistry treatment of the surface, the edges at the corners of this junction obtained high surface energy and were able to obstruct the movement of the droplet. When the air pressure difference applied to the droplet equaled the internal capillary pressure caused by the difference in the curvature between the two liquid-air interfaces of the droplet, the liquid-air interface at the junction could then protrude out of the microchannel and into the junction, and be steadily pinned along the edges; the shape of the other liquid-air interface, on the other hand, would depend on the static contact angle of the liquid on the channel material under homogeneous pneumatic pressure. A liquid microlens was thus formed out of the droplet. Varying the air pressure difference within a certain range could change the shape of the pinned liquid-air interface, thus tuning the focal length of the resulting microlens. With proper pneumatic controls, this microlens could be further moved within the microchannel at different pre-defined spots corresponding to individual junctions.

A typical design of the microchannel network would consist of a main fluidic channel, two air inlets with pneumatic pressure controls for the handling of fluids, and a lens channel, as shown in Figure 22 [18]. At the beginning, a DI water stream was introduced into the main channel. When the stream passed junction J1, syringe air pump S1 injected an air plug into air conduit AC1 to separate a water droplet from the main stream. This segmented water continued to advance until it arrived at junction J2, when a lens droplet was split into the lens channel. The size of the lens droplet could be controlled by air pressures, P_1 and P_2, from air conduits AC1 and AC2, respectively. Syringe air pump S2 dispensed another air plug into AC2 to adjust P_2. This lens droplet subsequently advanced in the lens channel, and then stopped at the edges of the corners of J3 with a pressure difference $\Delta P = P_1 - P_2$ (on the order of 100Pa) over the droplet. To sustain the microlens at these two edges, ΔP needed to be kept less than a critical pressure difference ΔP_C. During the formation of the microlens, valve V1 remained closed and V2 was opened to ambient air before a water droplet in the main channel arrived at it. The microlens could be removed by opening V1 and exert air pressure to squeeze the droplet into the reservoir. The microlens also could be reformed on demand following the same procedures as described above.

This approach of microlens offers much flexibility and reconfigurability in the operation. The authors also demonstrated that the liquid microlens could be moved from one junction to another within the lens channel and be tuned in focal length. When applying a ΔP larger than the critical pressure difference at junction J3, the microlens would leave J3. The lens droplet would then stop at J4 by immediately decreasing ΔP to less than the critical pressure difference at J4, ΔP_{J4}. The microlens at junctions J3 and J4 could both be tuned as well, while being stably pinned along the edges at the corners of the specific junction. At a ΔP larger than ΔP_{J4}, the microlens would break the geometrical obstruction at J4 and flow into a reservoir through AC2 and V1. The varying focal length controlled pneumatically controlled ranged from 1.5 to 8.9 mm. It was also shown that with proper pneumatic control, two microlenses could be defined at J3 and J4, respectively, while each could be tuned in focal length [110].

3.3.2. Hydrodynamically tunable optofluidic microlenses—Mao *et al.* demonstrated a hydrodynamically tunable optofluidic microlens [111]. The mechanism of this optofluidic tunable microlens is shown in Figure 24(a) and (b). The microlens was constructed from two fluids with different refractive indices, 5 M of calcium chloride ($CaCl_2$) solution ($n = 1.445$) and DI water ($n = 1.335$). Both fluids were injected into a microfluidic channel with a 90° bend. The injection of the two miscible fluids side by side resulted in an optically smooth, nearly vertical interface, due to the laminar flow that dominated in microfluidic channels. Upon entering the bend, the fluid experienced a centrifugal force along the curved trajectory. The fluid flowing in the middle of the channel here the flow velocity was the highest experienced a higher centrifugal force than the surrounding flow. As a result, a pair of secondary counter-rotating vortices located in the upper and lower halves of the cross-sectional plane of the channel was induced. The secondary vortical flow perturbed the fluidic interface, pulling the fluid in the middle of the channel towards the outer channel wall and sweeping the fluid at the top and bottom of the channel towards the inner channel wall. Consequently, the originally flat fluidic interface outward, creating a cylindrical microlens. The magnitude of the overall interface bowing was determined by the ratio of the inertial and centrifugal force to the viscous force. Therefore, the shape of the fluidic interface, and the optical characteristic of the cylindrical microlens, could be altered by changing the flow rate.

Using the simulated lens profiles, the authors further performed a ray-tracing simulation to calculate the focal length of the optofluidic microlens at different flow rates, as shown in Figure 24(c) [111]. A cone-shaped divergent light source was employed to simulate the input beam of the fiber. Three different flow rates (150, 250, and 350 □ min^{-1}) resulted in three focusing patterns, representing (i) under-focused, (ii) focused, and (iii) over-focused configurations.

3.3.3. Liquid-core/liquid-cladding microlens—Tang *et al.* [112] and Seow *et al.* [113] described the design and operation of another type of dynamically reconfigurable microfluidic lens for use in microfluidic networks. The lens was formed by laminar flow of three streams of fluids. The refractive index of the central (“core”) stream was higher than those of the sandwiching (“cladding”) streams. The streams entered a microchannel designed with a laterally expanded region. Figure 25 shows the working principle of the formation of this type of liquid microlenses with different lens curvatures in the expansion chamber by tuning the flow rates of the three liquid streams [113]. The configuration of the liquid lens was controlled hydrodynamically through the flow rates of the three streams. The central, core stream had a flow rate of V_{co}. The other two cladding streams, left and right, had flow rates of V_{cll} and V_{clr}, respectively. If $V_{cll} = V_{clr} < V_{co}$, a fluidic biconvex lens was formed. The two radii of curvature of the lens could be tuned individually with V_{cll}, V_{clr}, and V_{co}. The radii of curvature were increased when V_{cll} or V_{clr} increased. For example, when V_{clr} was increased and was higher than V_{co}, the radius of curvature of the right interface was increased. When the radius of curvature from the right side reached infinity, a planar convex lens was formed. When V_{clr} was further increased, a concave-convex lens was then formed. By varying the flow rates, the curvatures of the left and right interfaces were varied to obtain an extensive range of lens shapes: meniscus, plano-convex, and biconvex [113].

3.3.4. Hydrodynamically adjustable 3-dimensional optofluidic microlens—Rosenauer *et al.* demonstrated another approach to form an adjustable 3-dimensional (3D) optical lens with a single-layer, planar microfluidic device [114]. The approach was based on altering the flow rate within the channels. Figure 26 depicts the schematics in this work for the formation of a biconic optofluidic lens by using computational fluid dynamic (CFD) simulation. The analyzed microfluidic device design included three inlets for both the lens

body and cladding flows and one outlet. For each lens component, there were also two more 90° curved channels. By combining the single arch channels, a transversal multiconvex lens was generated. The lens body and the cladding fluid streams were then driven through a lateral expansion region where the flow was widened in the center to produce the3D characteristics of the optofluidic lens. By altering the flow rates in absolute values but maintaining a constant core to cladding ratio, the authors were able to reconfigure the transversal lens independently. The focal plane was adjustable in the *y*-direction as defined in Figure 26.

3.3.5. Air liquid interfacial microlens controlled by active pressure—Shi *et al.* demonstrated another optofluidic microlens by means of active pressure control of an air-liquid interface [115]. The working mechanism of this microlens is shown in Figure 27. DI water was introduced into a straight microchannel. The microchannel intersected an air reservoir through a T-junction. As the water flowed past the T-junction, air was trapped in the air reservoir and a movable air–water interface was thus formed at the T-junction, with the air bending into the water due to the air–liquid contact angle and the hydrophobic–hydrophilic interaction between the surface and the liquid. The air–water interface acted as a divergent lens. To focus light, a static, convergent polymer lens was coupled with the air-water lens. This polymer lens was made of PDMS and bent into an air gap. The focal length of the combination of the two lenses was tuned by adjusting the focal lens of the divergent fluidic lens, facilitated by altering the flow rate of the DI water in the straight microchannel. An increase in flow rate resulted in an increase in the radius of curvature of the air-water interface and an increase in the distance between the interface and the PDMS lens, as shown in Figure 27(b) to (e). These two factors had counteracting effects on the degree of divergence in the light incident on the PDMS lens, but the radius of curvature of the interface had a much stronger effect on the light divergence than the movement of the interface. Therefore, overall, an increased flow rate of the DI water resulted in a shorter image distance [115].

4. Conclusions

Microlenses have undergone rapid development in recent years, and have found many applications in many fields including imaging, especially biomedical imaging [1, 10–14], optical communication [15, 16], photolithography [2, 17], and LOC [3, 18–20]. Tunable microlenses, whose focal length can be adjusted on demand utilizing micro-scale actuators are of special interest for their added functionalities without complicated, extra actuation elements that would otherwise be a bottleneck for miniaturized optical systems. MEMS technologies have been widely applied to provide such micro-scale actuators to enable tunable microlenses. These tunable microlenses involving MEMS techniques can be mechanically or electrically driven. With the recent booming of LOC and microfluidic systems, tunable liquid lenses integrated within microfluidic channels, and especially those with optical axes parallel to the substrate, have caught much attention. Despite the promising progress in the development in these tunable microlenses involving MEMS techniques, many issues still remain for the researchers to tackle in the future. These issues include but are not limited to packaging, evaporation and leakage of liquids, characterization and improvement in the performance, such as filling factor, energy consumption, switching speed, stability and the optical parameters, and better integration with miniaturized optical system. Although gravity becomes less effective at the millimeter or sub-millimeter scale, for applications requiring strong mechanical robustness (e.g., shock resistance), the effect of inertia needs to be further addressed.

Acknowledgments

The preparation of this paper was partially supported by the US National Institute of Health (Grant No. 1D2OD008678-01) and the US National Science Foundation (Grant Nos. EFRI 0937847, ECCS 0745000). We thank A. Kanhere for her help in preparing the manuscript. We would also like to express our sincere regret s to all researchers whose relevant work could not be discussed owing to limited space.

References

1. Jeong KH, Kim J, Lee LP. Biologically inspired artificial compound eyes. Science. 2006; 312:557–61. [PubMed: 16645090]
2. Wu MH, Whitesides GM. Fabrication of diffractive and micro-optical elements using microlens projection lithography. Adv Mater. 2002; 14:1502–06.
3. Roulet JC, Völkel R, Herzig HP, Verpoorte E, de Rooij NF, Dändliker R. Fabrication of multilayer systems combining microfluidic and microoptical elements for fluorescence detection. J Microelectromech Syst. 2001; 10:482–91.
4. Moench W, Zappe H. Fabrication and testing of micro-lens arrays by all-liquid technique. J Opt A: Pure Appl Op. 2004; 6:330–7.
5. Wu MH, Whitesides GM. Fabrication of two-dimensional arrays of microlenses and their applications in photolithography. J Micromech Microeng. 2002; 12:747–58.
6. Jain A, Xie HK. An electrothermal microlens scanner with low-voltage large-vertical-displacement actuation. IEEE Photon Technol Lett. 2005; 17:1971–3.
7. Pan LW, Shen X, Lin L. Microplastic lens array fabricated by a hot intrusion process. J Microelectromech Syst. 2004; 13:1063–71.
8. Choo H, Muller RS. Addressable microlens array to impove dynamic range of Shack-Hartmann sensors. J Microelectromech Syst. 2006; 15:1555–67.
9. Wang, K.; Wei, KS.; Sinclair, M.; Böhringer, KF. Micro-optical components for a MEMS integrated display. The 12th Int. Workshop on The Physics of Semiconductor Devices; Chennai, India. 2003.
10. Duparré J, Dannberg P, Schreiber P, Bräuer A, Tünnermann A. Thin compound-eye camera. Appl Optics. 2005; 44:2949–56.
11. Kuiper S, Hendriks BHW. Variable-focus liquid lens for miniature cameras. Appl Phys Lett. 2004; 85:1128–30.
12. Chen S, Xinjian Y, Linbing K, Miao H, Hongchen W. Monolithic integration technique for microlens arrays with infrared focal plane arrays. Infrared Phys Technol. 2002; 43:109–12.
13. Stevens RF, Davies N, Milnethorpe G. Lens arrays and optical system for orthoscopic three-dimensional imaging. Imaging Sci J. 2001; 49:151–64.
14. Stevens RF, Harvey TG. Lens arrays for a three-dimensional imaging system. J Opt A: Pure Appl Op. 2002; 4:S17–21.
15. Hamam H. A two-way optical interconnection network using a single mode fiber array. Opt Commun. 1998; 150:270–6.
16. Eitel S, Fancey SJ, Gauggel HP, Gulden KH, Bachtold W, Taghizadeh MR. Highly uniform vertical-cavity surface-emitting lasers integrated with microlens arrays. IEEE Photon Technol Lett. 2000; 12:459–61.
17. Chang CY, Yang SY, Wu MS, Jiang LT, Wang LA. A novel method for fabrication of plastic microlens array with aperture stops for projection photolithography. Jpn J Appl Phys 1. 2007; 46:2932–5.
18. Dong L, Jiang H. Tunable and movable liquid microlens in situ fabricated within microfluidic channels. Appl Phys Lett. 2007; 91:041109.
19. Chronis N, Gang LL, Ki-Hun J, Luke LP. Tunable liquid-filled microlens array integrated with microfluidic network. Opt Express. 2003; 11:2370–8. [PubMed: 19471346]
20. Camou S, Fujita H, Fujii T. PDMS 2D optical lens integrated with microfluidic channels: principle and characterization. Lab Chip. 2003; 3:40–5. [PubMed: 15100804]

21. Aljasem K, Werber A, Seifert A, Zappe Hans. Fiber optic tunable probe for endoscopic optical coherence tomography. J Opt A: Pure Appl Op. 2008; 10:044012.
22. Huang D, Swanson EA, Lin CP, Schuman JS, Stinson WG, Chang W, Hee MR, Flotte T, Gregory K, Puliafito CA, Fujimoto JG. Optical Coherence Tomography. Science. 1991; 254:1178–81. [PubMed: 1957169]
23. Iftimia N, Bouma B, de Boer J, Park B, Cense B, Tearney G. Adaptive ranging for optical coherence tomography. Opt Express. 2004; 12:4025–34. [PubMed: 19483942]
24. Wang LV. Optical tomography for biomedical applications. IEEE Eng Med Biol Mag. 1998; 17:45–6. [PubMed: 9548080]
25. Zeng X, Smith CT, Gould JC, Heise CP, Jiang H. Fiber Endoscopes Utilizing Liquid Tunable-Focus Microlenses Actuated Through Infrared Light. J Microelectromech Syst. 2011; 20:583–93.
26. Völkel R, Eisner M, Weible KJ. Miniaturized imaging systems. Microelectron Eng. 2003; 67–68:461–72.
27. Gardner, JW.; Varadan, VK.; Awadelkarim, AO. Microsensors, MEMS, and Smart Devices. Chichester, UK: Wiley; 2001.
28. Franssila, S. Introduction to Micro Fabrication. Chichester, UK: Wiley; 2004.
29. Senturia, SD. Microsystem Design. Norwell, MA, USA: Kluwer Academic Publishers; 2001.
30. Kovacs, GTA. Micromachined Transducers Sourcebook. New York, NY, USA: McGraw-Hill; 1998.
31. Liu, C. Foundamentals of MEMS. 2. Upper Saddle River, NJ, USA: Prentice Hall; 2012.
32. Saliterman, SS. Fundamentals of BioMEMS and Medical Microdevices. Bellingham, WA, USA: SPIE; 2006.
33. Born, M.; Wolf, E. Principles of Optics. 6. New York, NY, USA: Cambridge University Press; 1998.
34. Ray, SF. Applied Photographic Optics. 3. Woburn, MA, USA: Focal Press; 2002.
35. Meyer-Arendt, JR. Introduction to Classical and Modern Optics. London: Prentice-Hall; 1972.
36. Zemax. Available from: http://en.wikipedia.org/wiki/Zemax
37. Lohmann AW. Scaling Laws for Lens Systems. Appl Optics. 1989; 28:4996–8.
38. Land, MF.; Nilsson, DE. Animal Eyes. New York, NY, USA: Oxford University Press; 2002.
39. Sze, SM. VLSI Technology. New York, NY, USA: McGraw-Hill; 1988.
40. Chang, CY.; Sze, SM. ULSI Technology. New York, NY, USA: McGraw-Hill; 1996.
41. Campbell, SA. The Science and Engineering of Microelectronic Fabrication. 2. New York, NY, USA: Oxford University Press; 2001.
42. Zant, PV. Microchip Fabrication: a Practical Guide to Semiconductor Processing. 4. New York, NY, USA: McGraw-Hill; 2000.
43. Plummer, JD.; Deal, MD.; Griffin, PB. Silicon VLSI Technology: Fundamentals, Practice and Modeling. Upper Saddle River, NJ, USA: Prentice Hall; 2000.
44. Xia YN, Whitesides GM. Soft lithography. Annu Rev Mater Sci. 1998; 28:153–84.
45. Tadmor R. Line energy and the relation between advancing, receding, and Young contact angles. Langmuir. 2004; 20:7659–64. [PubMed: 15323516]
46. Cheng DM, Choe YJP, Jiang HR. Controlled liquid-air interfaces and interfacial polymer micromembranes in microfluidic channels. J Microelectromech Syst. 2008; 17:962–73.
47. Liu Y, Aldalali B, Jiang H. Lateral tunable liquid microlenses for enhanced fluorescence emission in microfluidic channels. J Micromech Microeng. 2010; 22:105010.
48. Ren H, Xu S, Wu ST. Effects of gravity on the shape of liquid droplets. Opt Commun. 2010; 283:3255–8.
49. Mugele F, Baret JC. Electrowetting: from basics to applications. J Phys -Condens Mat. 2005; 17:R705.
50. Lei W, Huikai X. A Millimeter-Tunable-Range Microlens for Endoscopic Biomedical Imaging Applications. IEEE J Quantum Electron. 2010; 46:1237–44.
51. Ahn SH, Kim YK. Proposal of human eye's crystalline lens-like variable focusing lens. Sensor Actuat A-Phys. 1999; 78:48–53.

52. Zhang DY, Lien V, Berdichevsky Y, Choi J, Lo YH. Fluidic adaptive lens with high focal length tunability. Appl Phys Lett. 2003; 82:3171–2.
53. Werber A, Zappe H. Tunable microfluidic microlenses. Appl Optics. 2005; 44:3238–45.
54. Jeong KH, Liu G, Chronis N, Lee L. Tunable microdoublet lens array. Opt Express. 2004; 12:2494–500. [PubMed: 19475086]
55. Chen J, Wang W, Fang J, Varahramyan K. Variable-focusing microlens with microfluidic chip. J Micromech Microeng. 2004; 14:675–80.
56. Feng GH, Chou YC. Fabrication and characterization of optofluidic flexible meniscus-biconvex lens system. Sensor Actuat A-Phys. 2009; 156:342–9.
57. Agarwal M, Gunasekaran RA, Coane P, Varahramyan K. Polymer-based variable focal length microlens system. J Micromech Microeng. 2004; 14:1665–73.
58. Moran PM, Dharmatilleke S, Khaw AH, Tan KW, Chan ML, Rodriguez I. Fluidic lenses with variable focal length. Appl Phys Lett. 2006; 88:041120.
59. Yu HB, Zhou GY, Chau FS, Lee FW, Wang SH, Leung HM. A liquid-filled tunable double-focus microlens. Opt Express. 2009; 17:4782–90. [PubMed: 19293908]
60. Xiong GR, Han YH, Sun C, Sun LG, Han GZ, Gu ZZ. Liquid microlens with tunable focal length and light transmission. Appl Phys Lett. 2008; 92:241119.
61. Jiang, H.; Zeng, X. Microlenses: Properties, Fabrication and Liquid Lenses. Boca Raton, FL: CRC Press; 2013.
62. Ren H, Wu ST. Variable-focus liquid lens by changing aperture. Appl Phys Lett. 2005; 86:211107.
63. Ren H, Fox D, Anderson PA, Wu B, Wu ST. Tunable-focus liquid lens controlled using a servo motor. Opt Express. 2006; 14:8031–6. [PubMed: 19529173]
64. Ren H, Wu ST. Variable-focus liquid lens. Opt Express. 2007; 15:5931–6. [PubMed: 19546896]
65. Dong L, Agarwal AK, Beebe DJ, Jiang H. Adaptive liquid microlenses activated by stimuli-responsive hydrogels. Nature. 2006; 442:551–4. [PubMed: 16885981]
66. Dong L, Agarwal AK, Beebe DJ, Jiang H. Variable-focus liquid microlenses and microlens arrays actuated by thermoresponsive hydrogels. Adv Mater. 2007; 19:401–5.
67. Dong L, Jiang H. pH-adaptive microlenses using pinned liquid-liquid interfaces actuated by pH-responsive hydrogel. Appl Phys Lett. 2006; 89:211120.
68. Osada Y, Gong JP, Tanaka Y. Polymer gels. J Macromol Sci-Pol R. 2004; C44:87–112. *(Reprinted from* 1997 *Functional Monomers and Polymers,* 497–528).
69. Zeng X, Li C, Zhu D, Cho HJ, Jiang H. Tunable microlens arrays actuated by various thermo-responsive hydrogel structures. J Micromech Microeng. 2010; 20:115035.
70. Zeng X, Jiang H. Tunable liquid microlens actuated by infrared light-responsive hydrogel. Appl Phys Lett. 2008; 93:151101.
71. Moglia A, Menciassi A, Schurr MO, Dario P. Wireless capsule endoscopy: from diagnostic devices to multipurpose robotic systems. Biomed Microdevices. 2007; 9:235–43. [PubMed: 17160703]
72. Oleynikov D. Robotic Surgery. Surg Clin N Am. 2008; 88:1121–30. [PubMed: 18790158]
73. Knittela J, Schniedera L, Buessa G, Messerschmidtb B, Possnerb T. Endoscope-compatible confocal microscope using a gradient index-lens system. Opt Commun. 2001; 188:267–73.
74. Knittela J, Schniedera L, Buessa G, Messerschmidtb B, Possnerb T. Endoscope-compatible confocal microscope using a gradient index-lens system. Opt Commun. 2001; 188:267–73.
75. Zeng, X.; Jiang, H. An endoscope utilizing tunable-focus microlenses actuated through infrared light. The 15th Int. Conference on Solid-State Sensors, Actuators and Microsystems; Denver, CO, USA. 2009. p. 1214-7.
76. Corman, ML. Colon and Rectal Surgery. 5. Philadelphia: Lippincott Williams & Wilkins; 2005.
77. Zhu D, Li C, Zeng X, Jiang H. Tunable-focus microlens arrays on curved surfaces. Appl Phys Lett. 2010; 96:081111.
78. Zhu D, Zeng X, Li C, Jiang H. Focus-tunable microlens arrays fabricated on spherical surfaces. J Microelectromech Syst. 2011; 20:389–95.

79. Sato S. Liquid-Crystal Lens-Cells with Variable Focal Length. Jpn J Appl Phys. 1979; 18:1679–84.
80. Kowel ST, Cleverly DS, Kornreich PG. Focusing by Electrical Modulation of Refraction in a Liquid-Crystal Cell. Appl Optics. 1984; 23:278–89.
81. Kowel ST, Kornreich P, Nouhi A. Adaptive Spherical Lens. Appl Optics. 1984; 23:2774–7.
82. Nose T, Masuda S, Sato S. A Liquid-Crystal Microlens with Hole-Patterned Electrodes on Both Substrates. Jpn J Appl Phys 1. 1992; 31:1643–6.
83. Choi Y, Park JH, Kim JH, Lee SD. Fabrication of a focal length variable microlens array based on a nematic liquid crystal. Opt Mater. 2003; 21:643–6.
84. Riza NA, Dejule MC. Three-terminal adaptive nematic liquid-crystal lens device. Opt Lett. 1994; 19:1013–5. [PubMed: 19844517]
85. Cheng CC, Chang CA, Liu CH, Yeh JA. A tunable liquid-crystal microlens with hybrid alignment. J Opt A: Pure Appl Op. 2006; 8:S365–9.
86. Cheng CC, Chang CA, Yeh JA. Variable focus dielectric liquid droplet lens. Opt Express. 2006; 14:4101–6. [PubMed: 19516558]
87. Ren H, Fan YH, Wu ST. Liquid-crystal microlens arrays using patterned polymer networks. Opt Lett. 2004; 29:1608–10. [PubMed: 15309834]
88. Ren H, Fan YH, Wu ST. Tunable Fresnel lens using nanoscale polymer-dispersed liquid crystals. Appl Phys Lett. 2003; 83:1515–7.
89. Li G, Valley P, Giridhar MS, Mathine DL, Meredith G, Haddock JN, Kippelen B, Peyghambarian N. Large-aperture switchable thin diffractive lens with interleaved electrode patterns. Appl Phys Lett. 2006; 89:141120.
90. Scharf, T. Polarized Light in Liquid Crystals and Polymers. New York: Wiley Interscience; 2006.
91. Binh-Khiem N, Matsumoto K, Shimoyama I. Polymer thin film deposited on liquid for varifocal encapsulated liquid lenses. Appl Phys Lett. 2008; 93:124101.
92. Cheng CC, Yeh JA. Dielectrically actuated liquid lens. Opt Express. 2007; 15:7140–5. [PubMed: 19547032]
93. Ren H, Wu ST. Tunable-focus liquid microlens array using dielectrophoretic effect. Opt Express. 2008; 16:2646–52. [PubMed: 18542348]
94. Zeng XF, Yue RF, Wu JG, Dong L, Liu LT. Actuation and control of droplets by using electrowetting-on-dielectric. Chinese Phys Lett. 2004; 21:1851–4.
95. Gorman CB, Biebuyck HA, Whitesides GM. Control of the Shape of Liquid Lenses on a Modified Gold Surface Using an Applied Electrical Potential across a Self-Assembled Monolayer. Langmuir. 1995; 11:2242–6.
96. Berge B, Peseux J. Variable focal lens controlled by an external voltage: An application of electrowetting. Eur Phys J. 2000; 3:159–63.
97. Krupenkin T, Yang S, Mach P. Tunable liquid microlens. Appl Phys Lett. 2003; 82:316–8.
98. de Gennes PG. Wetting: statics and dynamics. Rev Mod Phys. 1985; 57:827.
99. Yang S, Krupenkin TN, Mach P, Chandross EA. Tunable and latchable liquid microlens with photopolymerizable components. Adv Mater. 2003; 15:940–3.
100. Li C, Jiang H. Electrowetting-driven variable-focus microlens on flexible surfaces. Appl Phys Lett. 2012; 100:231105. [PubMed: 22904571]
101. Lopez CA, Lee CC, Hirsa AH. Electrochemically activated adaptive liquid lens. Appl Phys Lett. 2005; 87:134102.
102. Gallardo BS, Gupta VK, Eagerton FD, Jong LI, Craig VS, Shah RR, Abbott NL. Electrochemical principles for active control of liquids on submillimeter scales. Science. 1999; 283:57–60. [PubMed: 9872739]
103. Takiguchi H, Odake T, Ozaki M, Umemura T, Tsunoda K. Liquid/liquid optical waveguides using sheath flow as a new tool for liquid/liquid interfacial measurements. Appl Spectrosc. 2003; 57:1039–41. [PubMed: 14661848]
104. Wolfe DB, Conroy RS, Garstecki P, Mayers BT, Fischbach MA, Paul KE, Prentiss M, Whitesides GM. Dynamic control of liquid-core/liquid-cladding optical waveguides. Proc of the National Academy of Sciences of the United States of America. 2004; 101:12434–8.

105. Kim JY, Jeong KH, Lee LP. Artificial ommatidia by self-aligned microlenses and waveguides. Opt Lett. 2005; 30:5–7. [PubMed: 15648619]

106. Chang-Yen DA, Eich RK, Gale BK. A monolithic PDMS waveguide system fabricated using soft-lithography techniques. J Lightwave Technol. 2005; 23:2088–93.

107. Conroy RS, Mayers BT, Vezenov DV, Wolfe DB, Prentiss MG, Whitesides GM. Optical waveguiding in suspensions of dielectric particles. Appl Optics. 2005; 44:7853–7.

108. Tang SKY, Mayers BT, Vezenov DV, Whitesides GM. Optical waveguiding using thermal gradients across homogeneous liquids in microfluidic channels. Appl Phys Lett. 2006; 88:061112.

109. Vezenov DV, Mayers BT, Wolfe DB, Whitesides GM. Integrated fluorescent light source for optofluidic applications. Appl Phys Lett. 2005; 86:041104.

110. Dong L, Jiang H. Selective formation and removal of liquid microlenses at predetermined locations within microfluidics through pneumatic control. J Microelectromech Syst. 2008; 17:381–92.

111. Mao X, Waldeisen JR, Juluri BK, Huang TJ. Hydrodynamically tunable optofluidic cylindrical microlens. Lab Chip. 2007; 7:1303–8. [PubMed: 17896014]

112. Tang SKY, Stan CA, Whitesides GM. Dynamically reconfigurable liquid-core liquid-cladding lens in a microfluidic channel. Lab Chip. 2008; 8:395–401. [PubMed: 18305856]

113. Seow YC, Liu AQ, Chin LK, Li XC, Huang HJ, Cheng TH, Zhou XQ. Different curvatures of tunable liquid microlens via the control of laminar flow rate. Appl Phys Lett. 2008; 93:084101–3.

114. Rosenauer M, Vellekoop MJ. 3D fluidic lens shaping-A multiconvex hydrodynamically adjustable optofluidic microlens. Lab Chip. 2009; 9:1040–2. [PubMed: 19350083]

115. Shi J, Stratton Z, Lin S-CS, Huang H, Huang TJ. Tunable optofluidic microlens through active pressure control of an air–liquid interface. Microfluid Nanofluid. 2010; 9:313–8.

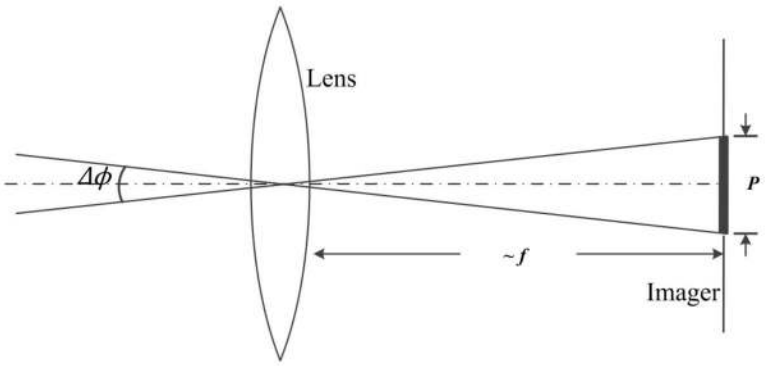

Figure 1.
Schematic of a microlens coupled with a CCD imager. Inter-receptor angle ΔΦ could be a performance limiting factor.

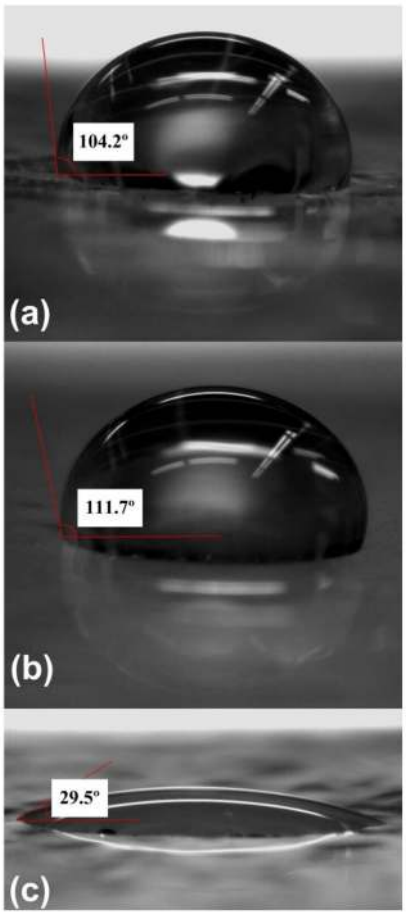

Figure 2.
Water droplets on (a) a native PDMS surface, (b) a PDMS surface coated with OTS, and (c) a PDMS surface treated with oxygen plasma. Measured contact angles are shown.

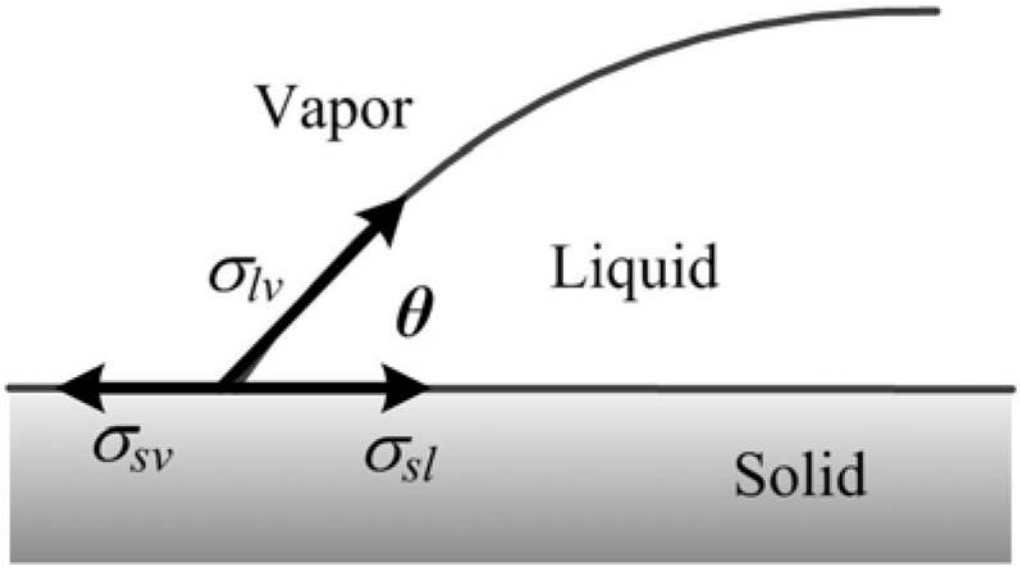

Figure 3.
Schematic showing the boundary of a liquid droplet on a solid surface. γ_{sv}, γ_{sl} and γ_{lv} are surface tensions of two phases solid-vapor, solid-liquid and liquid-vapor, respectively. θ is the contact angle between solid and liquid.

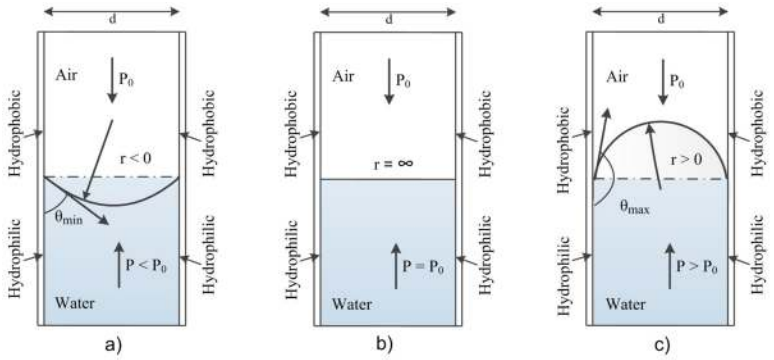

Figure 4.

Controlling the pressure difference across a water to air interface in a tube can generate a water meniscus with different radius of curvature, resulting in a lens with tunable focal length. The top half of the inner surface is hydrophobic and the bottom half hydrophilic. A water meniscus is pinned at the hydrophobic-hydrophilic boundary. Different air-liquid interfaces with an applied pressure a) $P < P_0$, b) $P = P_0$, and c) $P > P_0$, where P_0 is atmosphere pressure, represent a concave, flat and convex lens, respectively. r and θ are radius of curvature and contact angle of air-liquid interface, respectively.

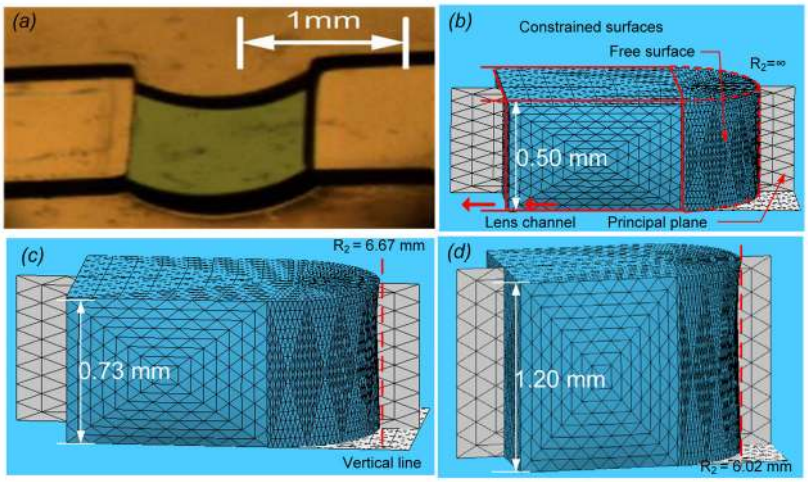

Figure 5.

(a) The effect of gravity on cylindrical liquid microlenses formed by a water droplet protruding out of a junction in a microfluidic channel (channel walls not shown). Simulated steady-state shapes of the of cylindrical microlenses with different heights are shown: (b) 0.50 mm, (c) 0.73 mm, (d) 1.20 mm. The distortion of the free lens surface is depicted by the principal plane intersecting the surface, and comparing the intersecting line with a line perpendicular to the substrate. Reprinted from [47] with permission from *Institute of Physics.*

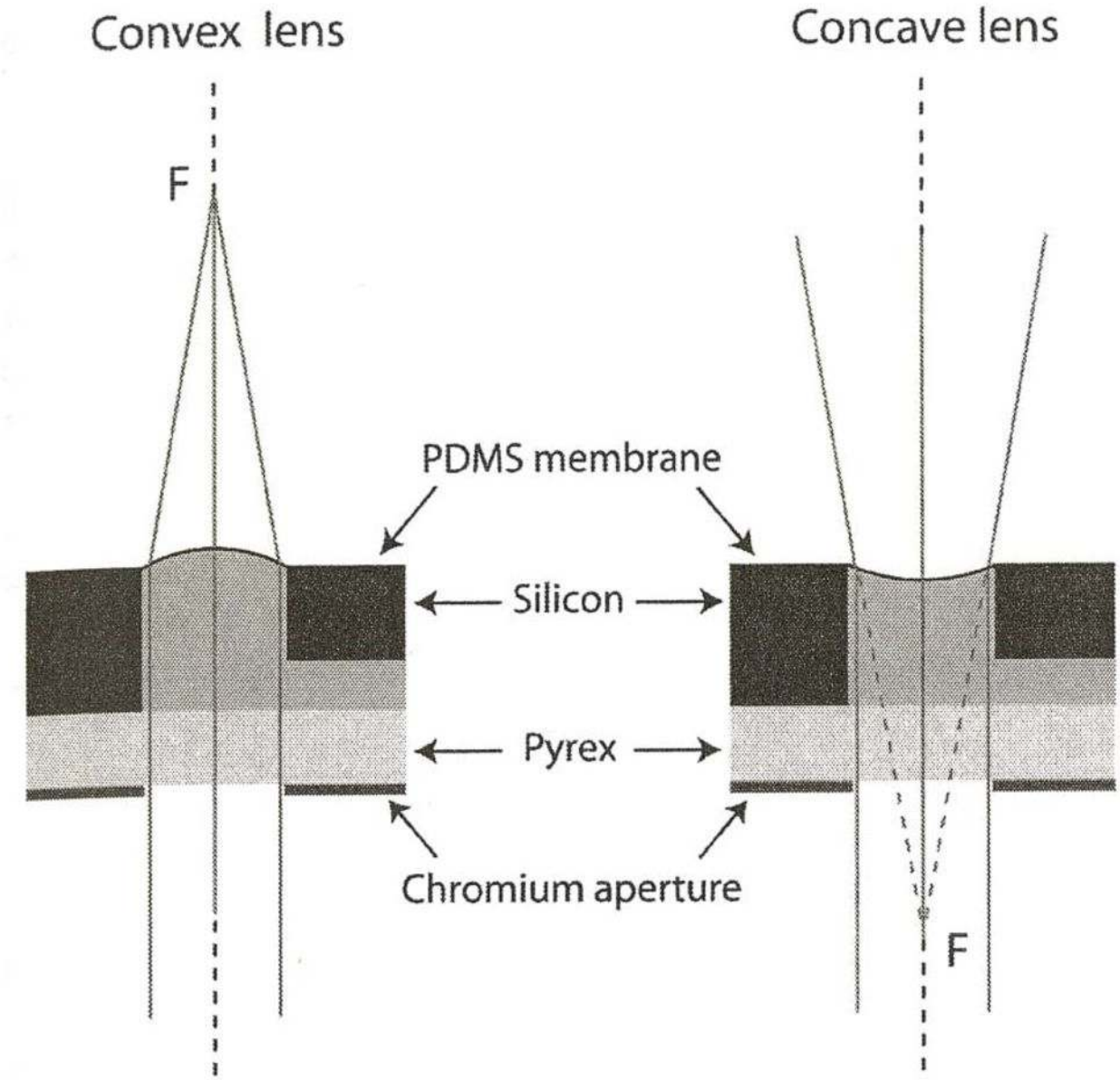

Figure 6.
Cross-sectional diagram of a tunable microlens through pneumatic pressure covered with a PDMS membrane, showing its implementation as plano–convex and plano–concave lenses. Reprinted from [53] with permission from *Optical Society of America*.

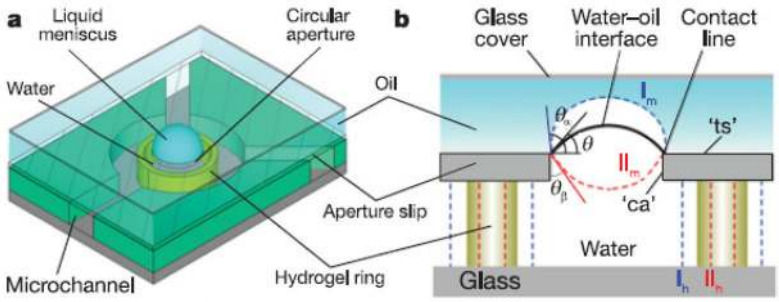

Figure 7.

(a) 3-dimensional schematic showing a water–oil interface that forms a liquid microlens. The microchannels allow the flow of fluids to the microlens structure. (b) The variable-focus mechanism. The hydrophilic sidewall and bottom surface and hydrophobic top surface of the aperture pin a water–oil meniscus along the edge. The expansion and contraction of the hydrogel regulates the shape of the liquid meniscus by changing the angle of the pinned water–oil interface to the edge. Reprinted from [65] with permission from *Nature Publishing Group*.

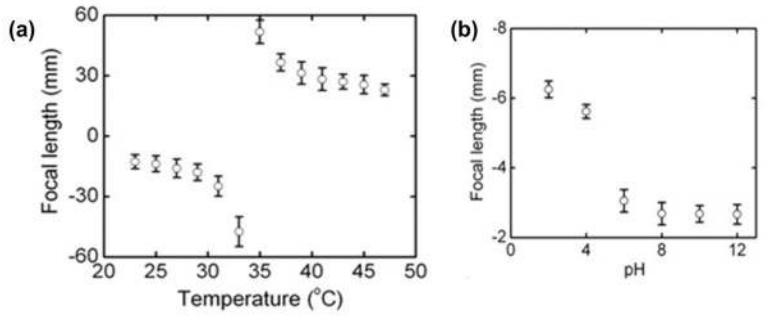

Figure 8.

(a) The focal length of a temperature-responsive liquid microlens as a function of temperature. The microlens is divergent between 23.8°C (focal length = −11.7 mm) and 33.8°C (focal length approaches – ∞). Between 33.8°C and 47.8°C, the microlens becomes convergent with a positive focal length from + ∞ to 22.8 mm. (b) The focal length of a pH-responsive liquid microlens utilizing AA hydrogel as a function of pH. Reprinted from [65] with permission from *Nature Publishing Group*.

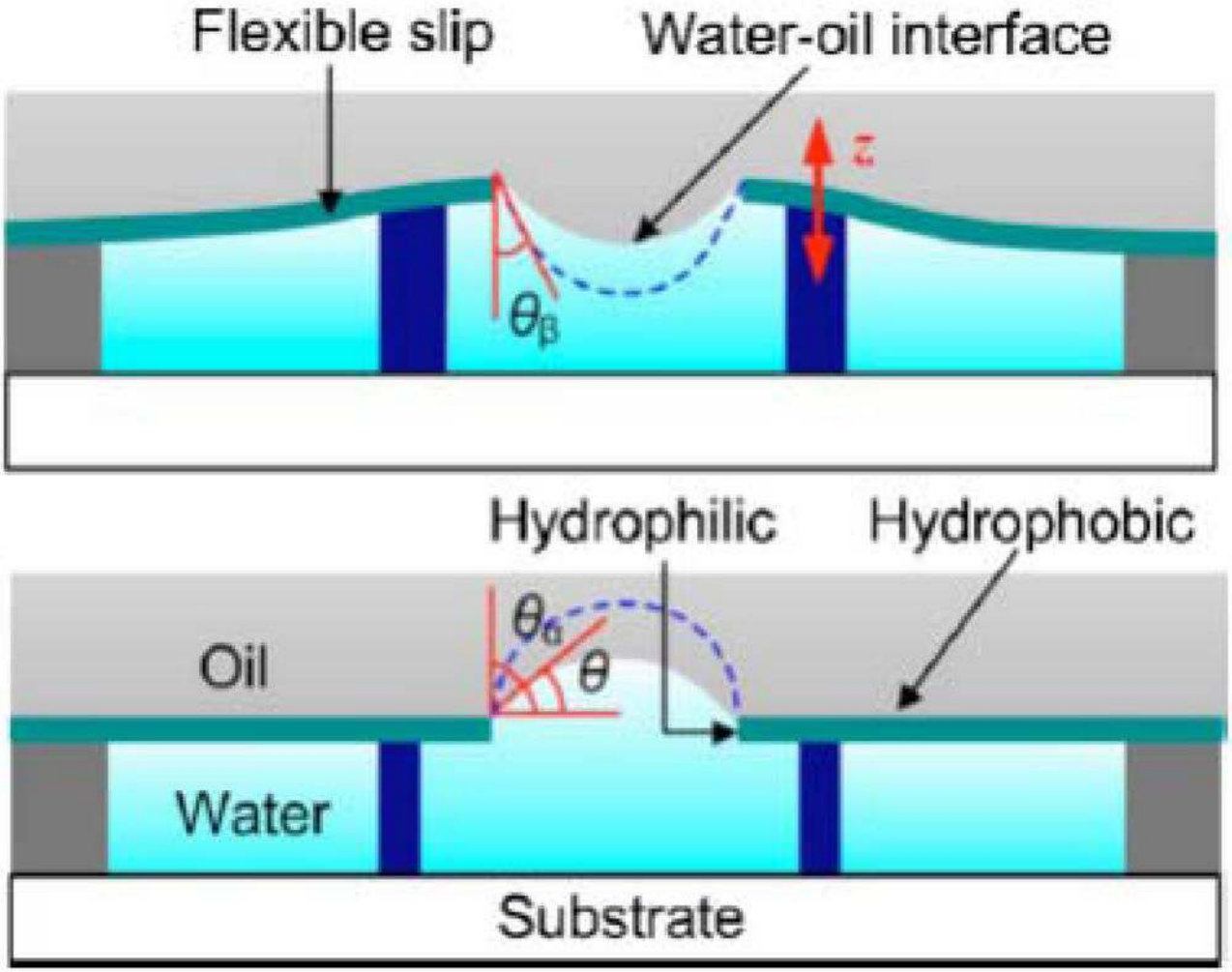

Figure 9.
A microlens is formed via an interface between oil and an aqueous solution. The interface is pinned stably at a hydrophobic-hydrophilic boundary along a circular aperture. The volumetric change of hydrogel microposts causes a flexible aperture slip to bend in the *z* direction. The pinned water-oil interface is pressed downward or upward, thus tuning the focal length of the microlens. Reprinted from [67] with permission from *American Institute of Physics*.

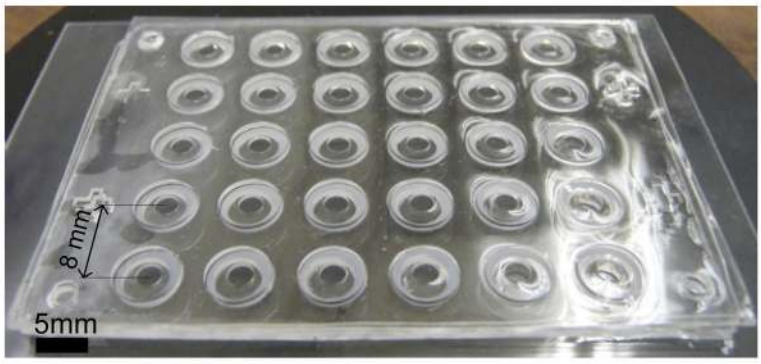

Figure 10.
Optical image of the structure of one microlens array without filling the lens liquids. The array consists of 5×6 microlenses. Reprinted from [69] with permission from *Institute of Physics*.

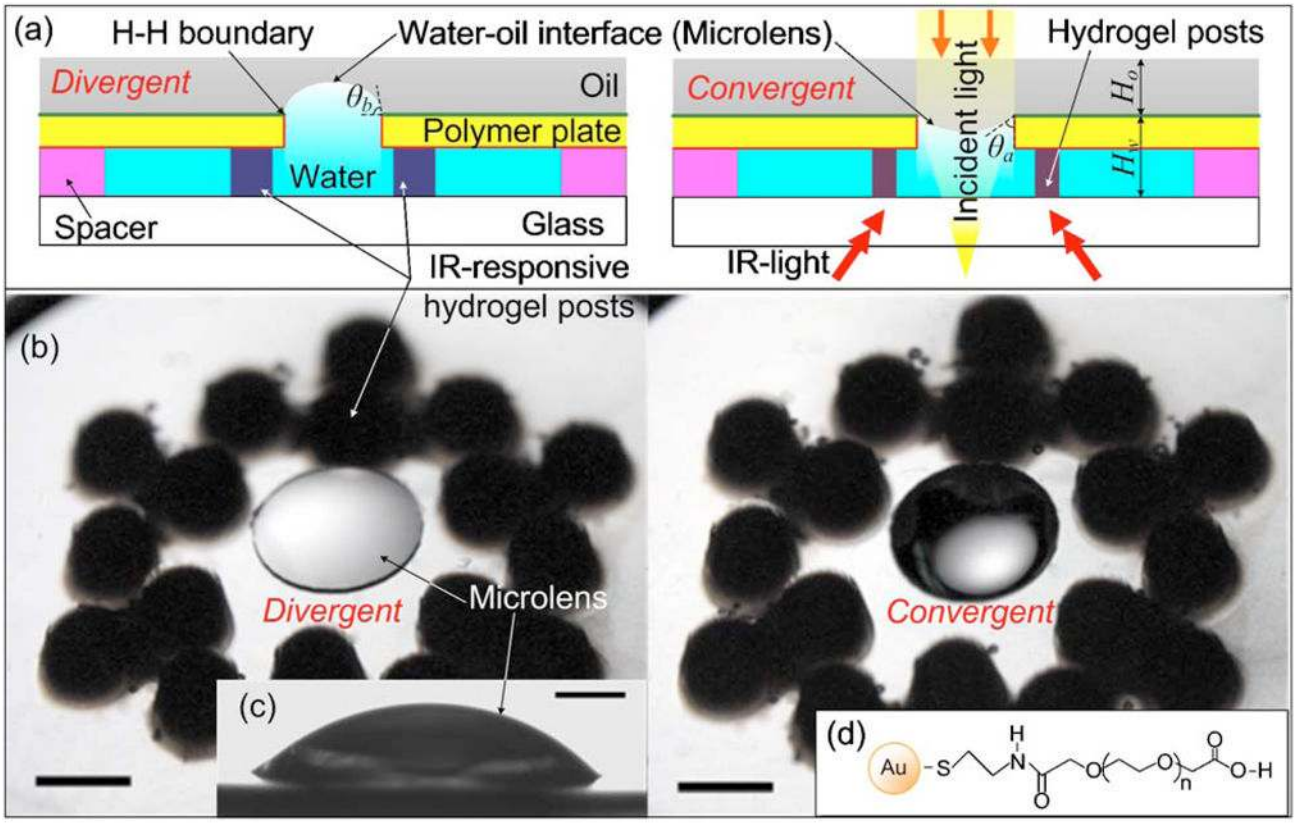

Figure 11.

Schematics and optical images of an IR light-actuated tunable liquid microlens. (a) Schematics of the microlens when it is divergent and convergent, respectively. (b) Optical images of such a microlens with 18 hydrogel microposts in divergent and convergent states, respectively. (c) Side profile of the water meniscus of the microlens in the divergent status at the starting point. The scale bars represent 1 mm. (d) Chemical structure of the gold nanoparticles coated with thiolated poly(ethylene glycol) ligands. Reprinted from [70] with permission from *American Institute of Physics*.

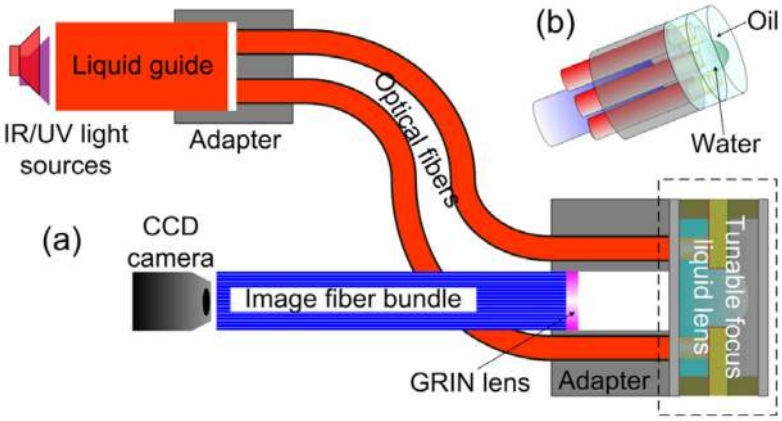

Figure 12.

(a) Schematic and (b) 3-dimensional schematic of a prototype endoscope with a liquid tunable-focus microlens integrated at its end and actuated through IR light. Two sets of optical fibers are used: the actuation fibers and the image acquisition fiber bundle. IR light is transmitted via the actuation optical fibers to tune the focal length of the microlens at the end of the fibers. Images from the microlens are transferred to a camera via the image acquisition fiber bundle. Reprinted from [25] with permission from *IEEE*.

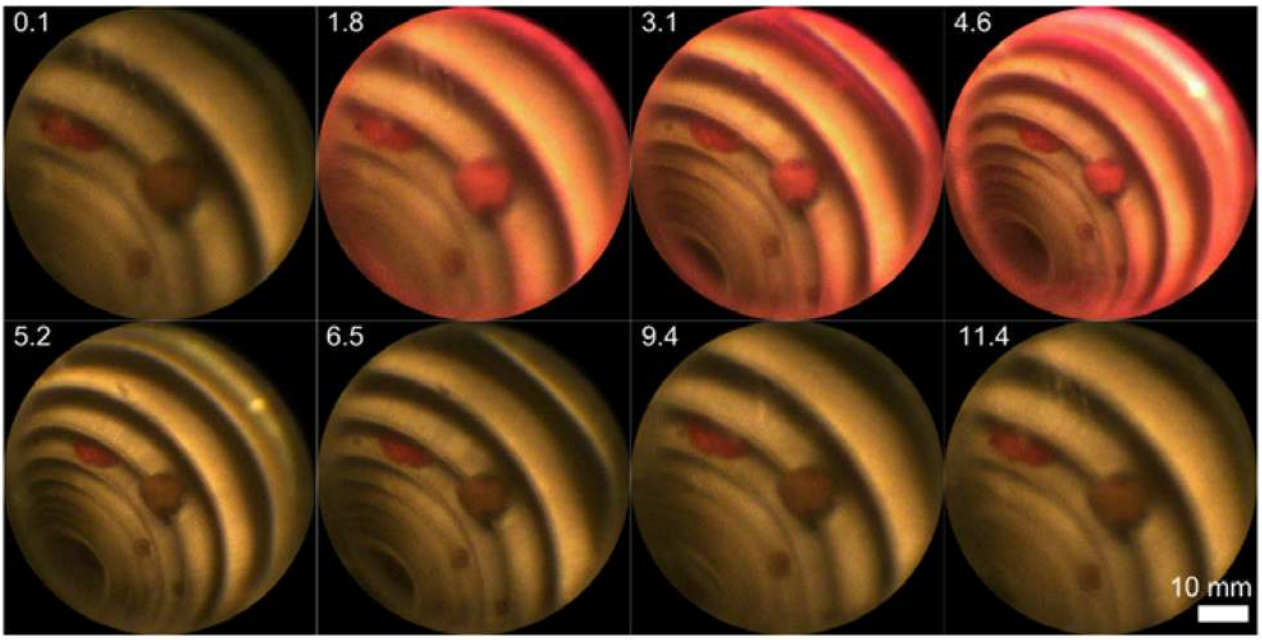

Figure 13.
Frame sequence of the focused images of a simulated human colon and polyps obtained from a prototype endoscope incorporating an IR-light-responsive tunable liquid microlens in one scanning cycle. Initially, three polyps could be observed in the field. From the time instant of 1.8 s, IR light was on and the angle of view (AOV) began to increase. At the time instant of 4.6 s, one extra polyp at the other end of the simulated colon lumen could be observed in the field. From the time instant of 5.2 s, IR light was off and the AOV of the microlens began to decrease. At the time instant of 11.4 s, the microlens went back to its original status. Reprinted from [25] with permission from *IEEE*.

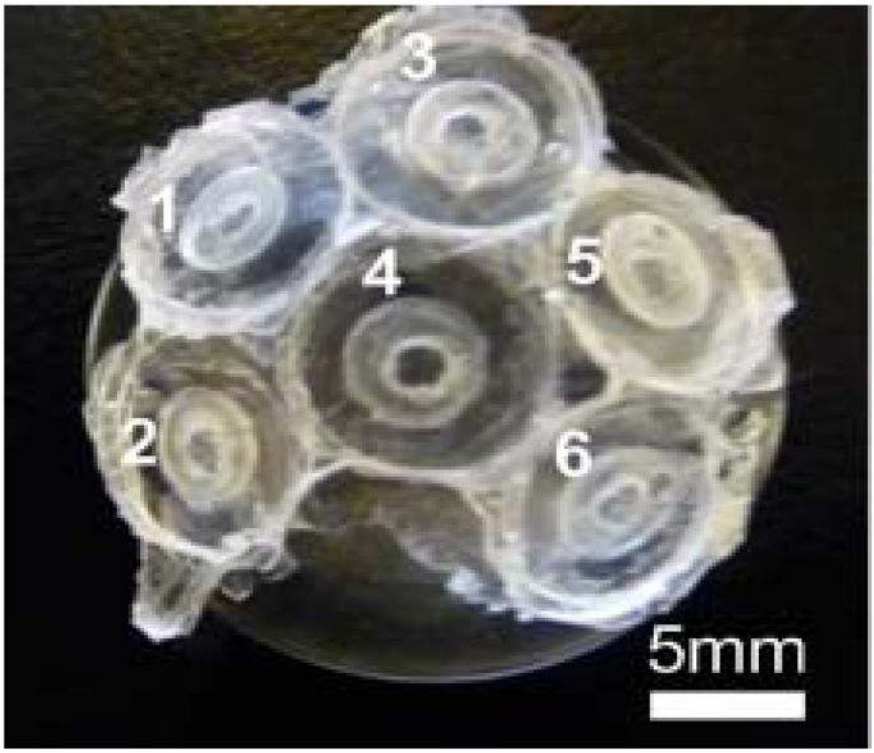

Figure 14.
A tunable liquid microlens array fabricated on a hemisphere. The lenses are individually tunable in their focal length. Reprinted from [78] with permission from *IEEE*.

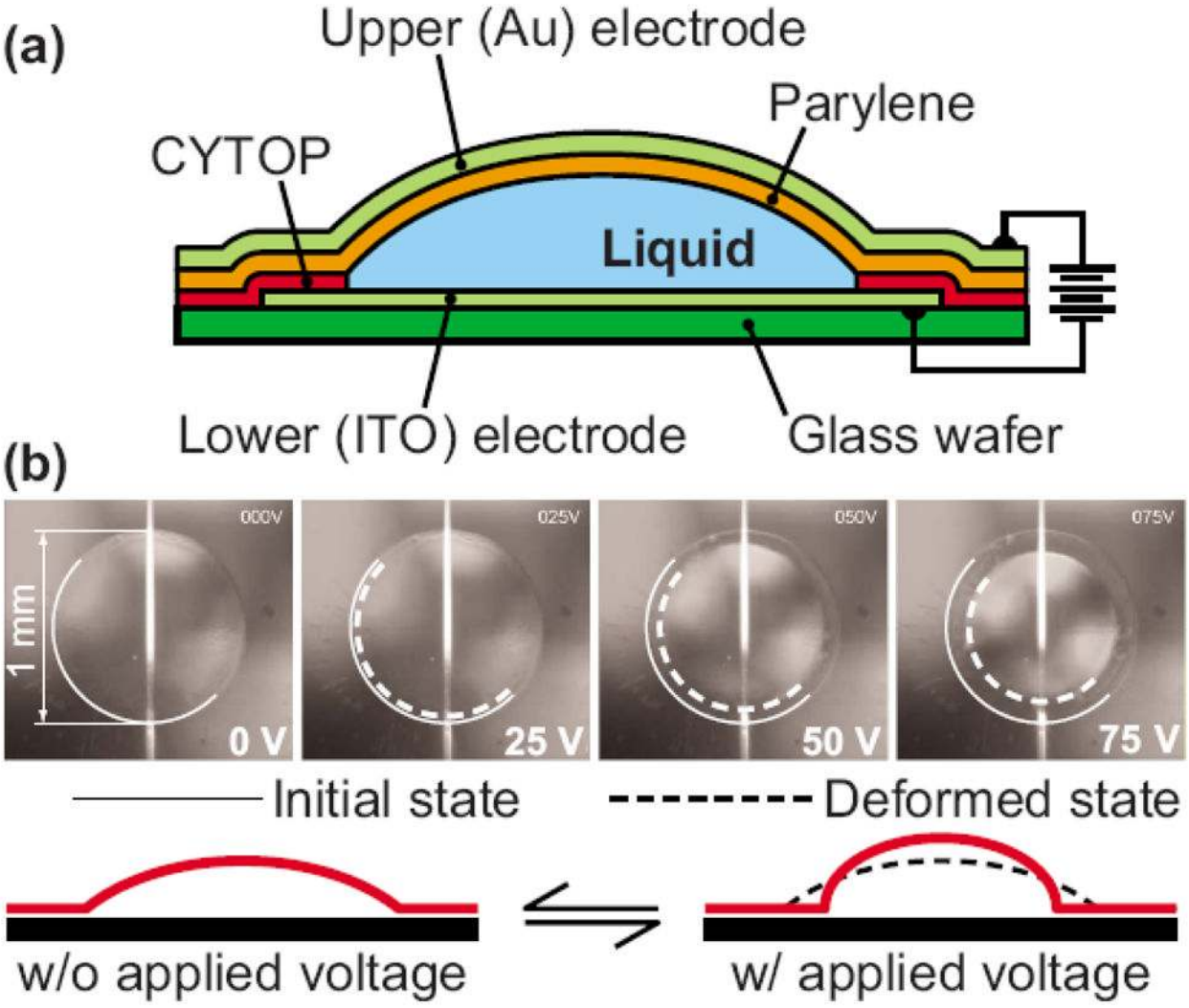

Figure 15.
Conceptual structure and deformation of a liquid lens packaged in a parylene thin film. (a) Lens conceptual structure. (b) Deformation of the lens shape upon applying voltage. Reprinted from [91] with permission from *American Institute of Physics*.

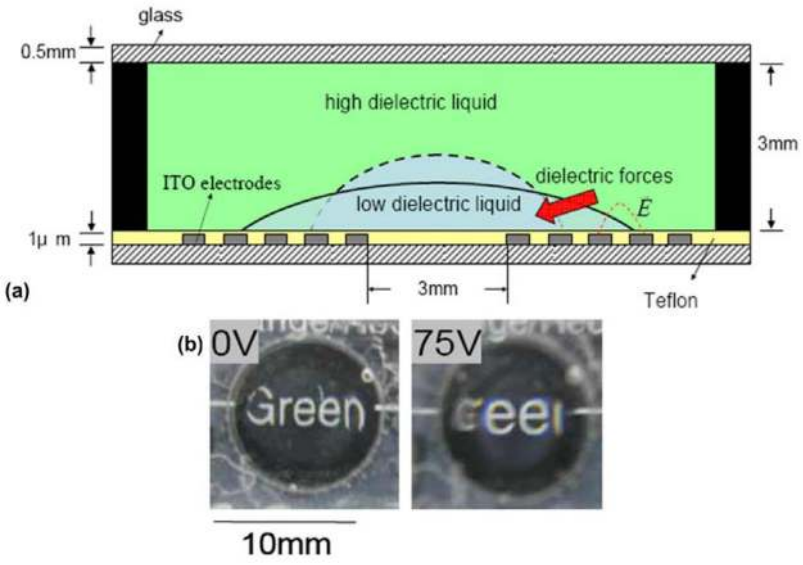

Figure 16.

(a) Illustration of a dielectric liquid lens. The droplet shrinks to a new state (dashed line) due to the dielectric force. (b) The captured images of an actuated liquid lens at the rest state (left) and at 75 volts (right). With the applied voltage across the electrodes, the dielectric force was exerted onto the droplet and shrank the droplet, increasing the contact angle of the droplet on the glass surface and shortening the focal length of the liquid lens. Reprinted from [92] with permission from *Optical Society of America*.

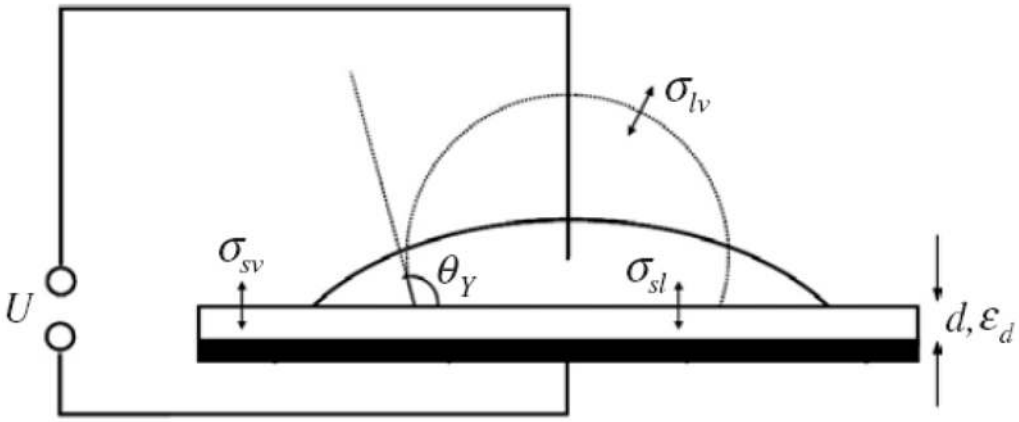

Figure 17.
A generic electrowetting set-up. Partially wetting liquid droplet at zero voltage (with contact angle of θ_Y) and at high voltage, respectively. Reprinted from [49] with permission from *Institute of Physics*.

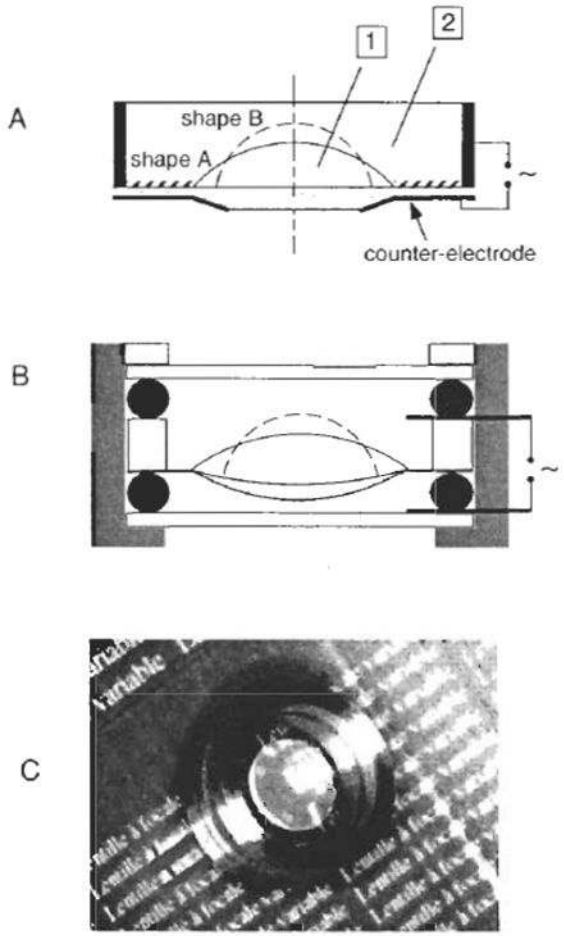

Figure 18.

(a) Schematic representation of a liquid lens using electrowetting (drawing not to scale). The cell is filled with water. A drop of an insulating and non-polar liquid is deposited on the bottom wall, which is made of an insulating and transparent material. The central disc on the bottom wall surface is hydrophobic in order to trap the drop. The outer zone is hydrophilic. The optical axis is shown as a short-long-dashed line. (b) The realization of the variable-focus liquid lens. The cell is sealed by o-rings. The central part has a diameter of 5 mm. (c) Photograph of one sample: the diameter of the stainless steel outer case is about 12 mm and the oil drop can be seen as white at the center of the case. Reprinted from [96] with permission from *Springer*.

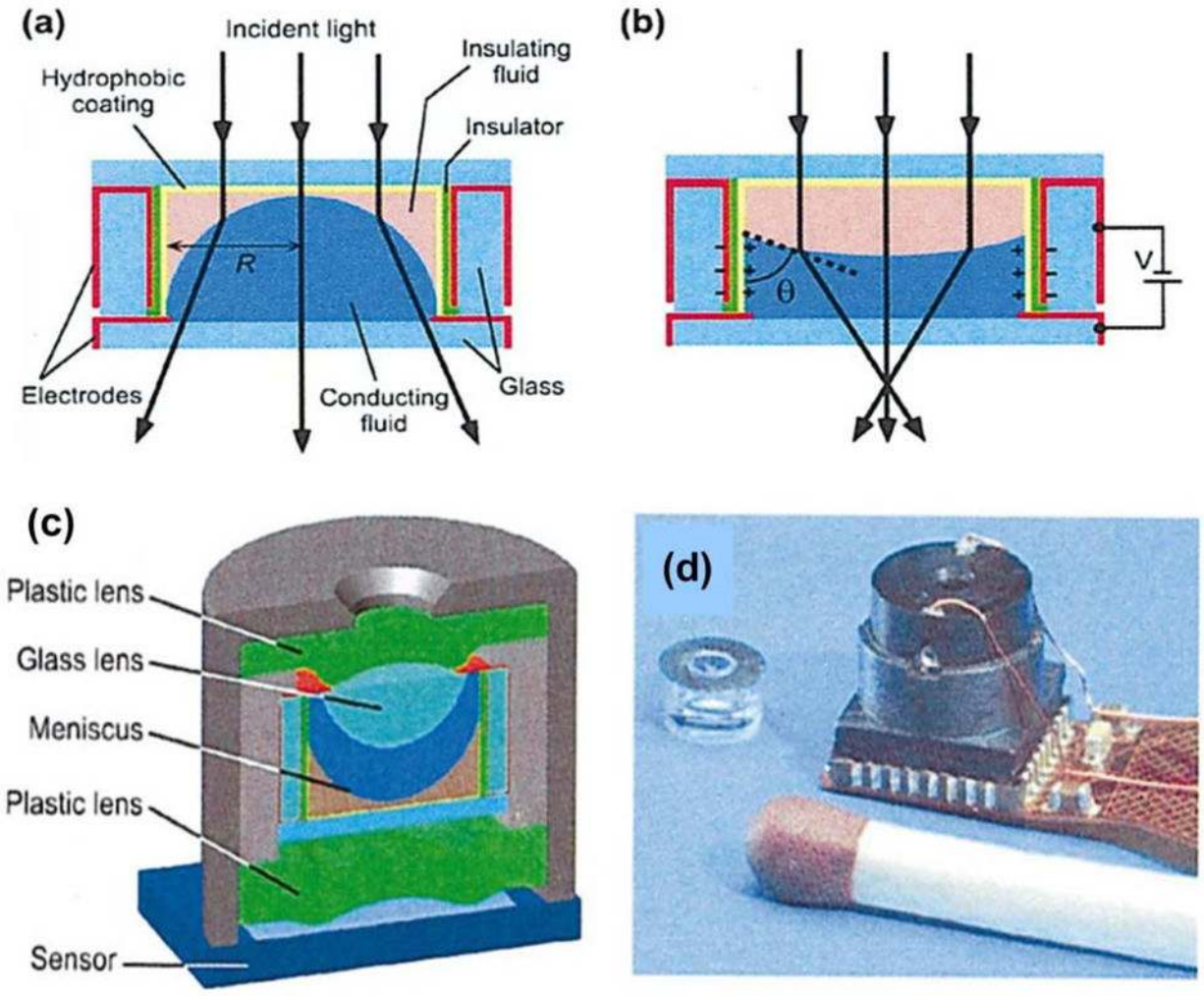

Figure 19.

(a) Schematic cross section of an electrowetting based variable lens in a cylindrical glass housing. The transparent electrodes are formed of 50-nm-thick ITO, the insulator was a 3- μm-parylene layer, and the 10-nm-hydrophobic top coating was a dip-coated fluoropolymer AF1600, supplied by Dupont. The top and bottom glass plates were glued onto the glass cylinder with epoxy glue. (b) When a voltage was applied, charges accumulated in the wall electrode and opposite charges collected near the solid/liquid interface in the conducting liquid. The resulting electrostatic force effectively lowered the solid–liquid interfacial tension and with that the contact angle □(c) Optical design of the camera module containing a liquid lens. (d) The assembled camera module and the liquid lens. Reprinted from [11] with permission from *American Institute of Physics*.

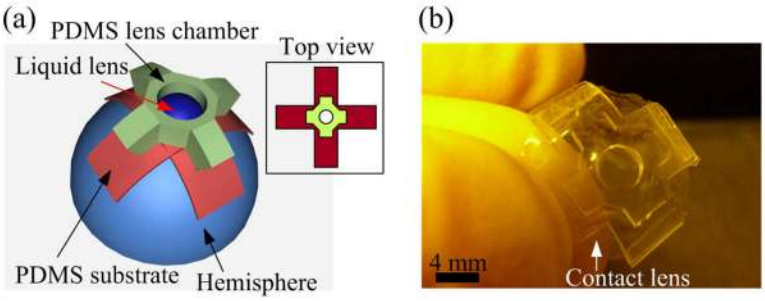

Figure 20.
(a) An electrowetting-based liquid lens fabricated on a curved surface. (b) Such a lens made on a commercial contact lens. Reprinted from [100] with permission from *American Institute of Physics*.

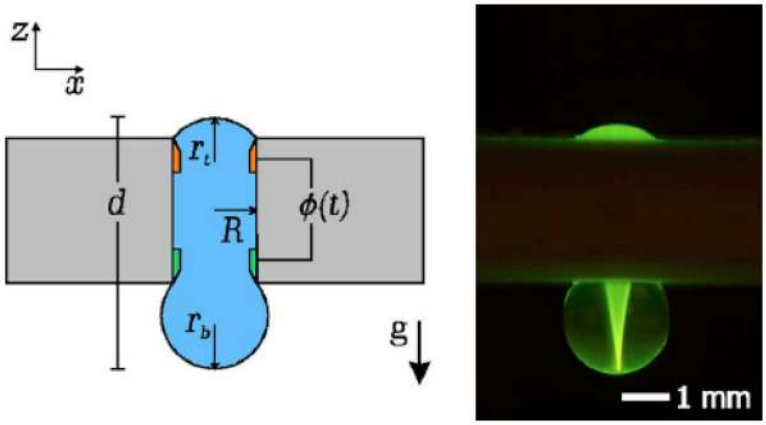

Figure 21.
Schematic of an electrochemically driven liquid lens showing the electrode embedded at each contact circle. The photo on the right was taken with a thin laser light sheet illuminating the liquid lens from above. For visualization, fluorescein dye at a 4 ppm concentration was dissolved in double-distilled water. Reprinted from [101] with permission from American *Institute of Physics*.

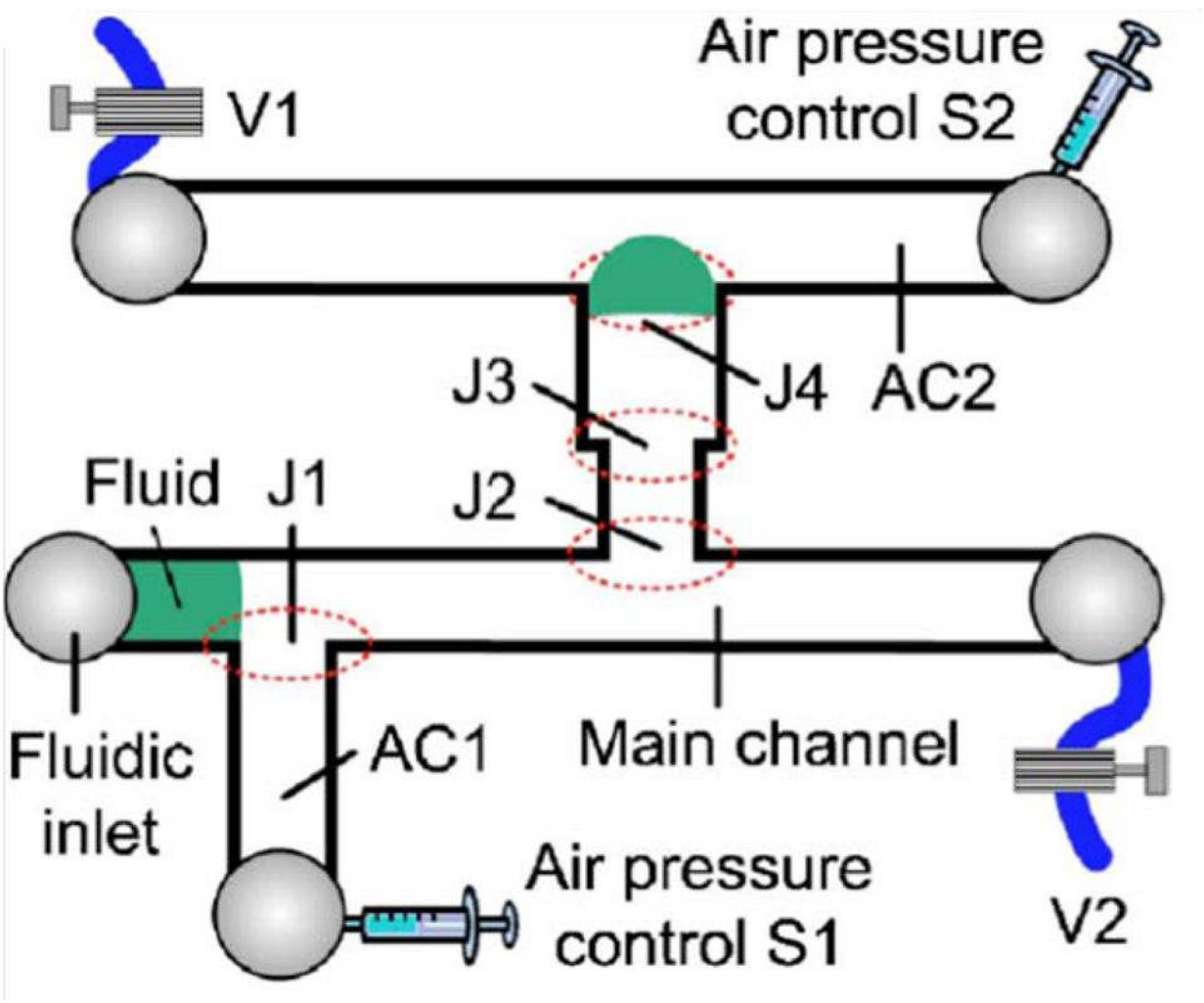

Figure 22.
Schematic of a microfluidic setup for the *in situ* formation of a liquid-droplet-based microlens. To realize the movement of a microlens from one junction to another, a small step is produced at junction J3. Reprinted from [18] with permission from *American Institute of Physics*.

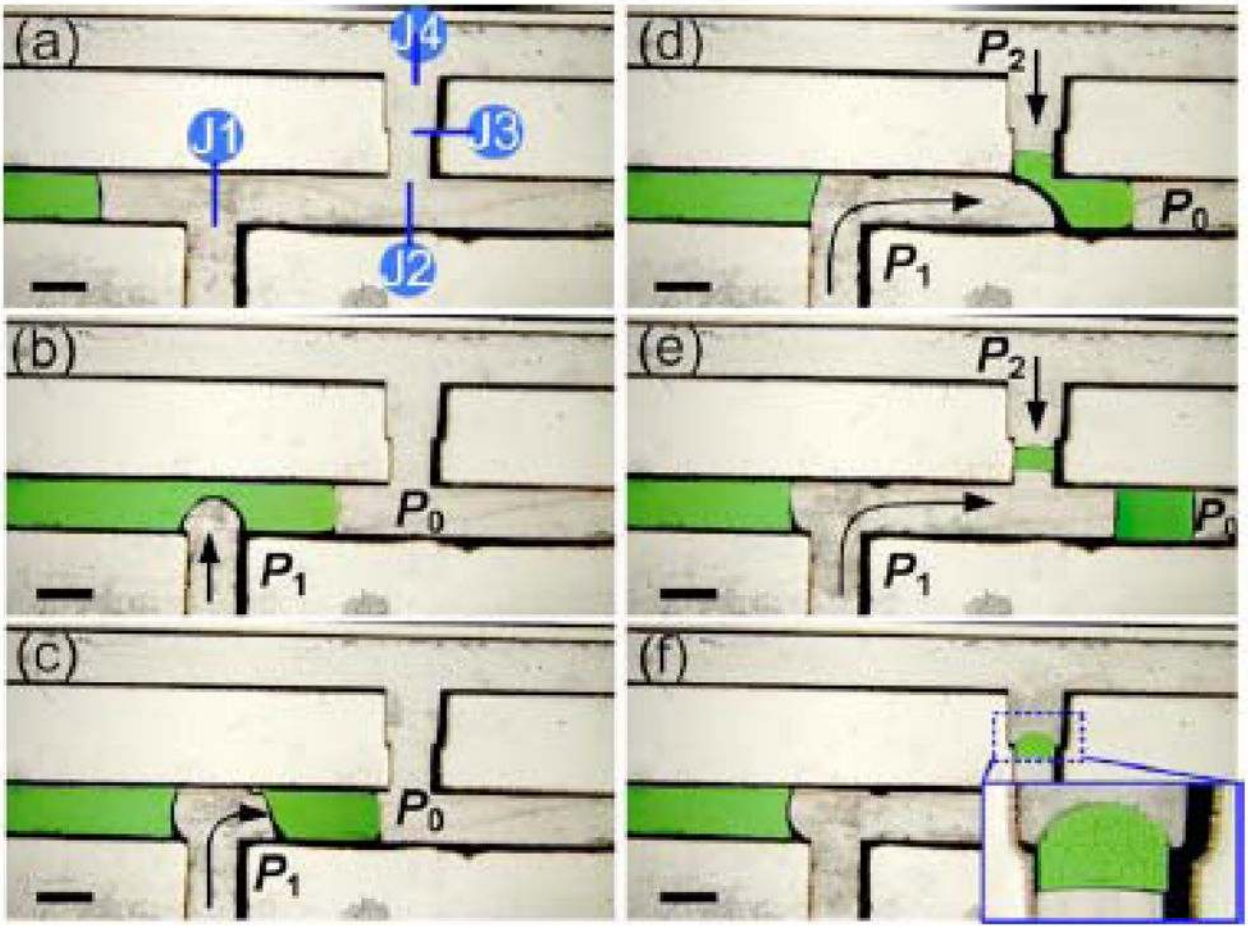

Figure 23.

In situ fabrication process of a liquid-droplet based microlens within a microchannel. (a) A stream is flowed into the main channel. (b) and (c) A water droplet is cut out of the main stream by air pressure P1 at junction J1. (d) and (e) A lens droplet is split into the lens channel at junction J2. (f) The lens droplet stops at junction J3. P0 denotes atmospheric pressure. Scale bars: 1 mm. Reprinted from [18] with permission from *American Institute of Physics*.

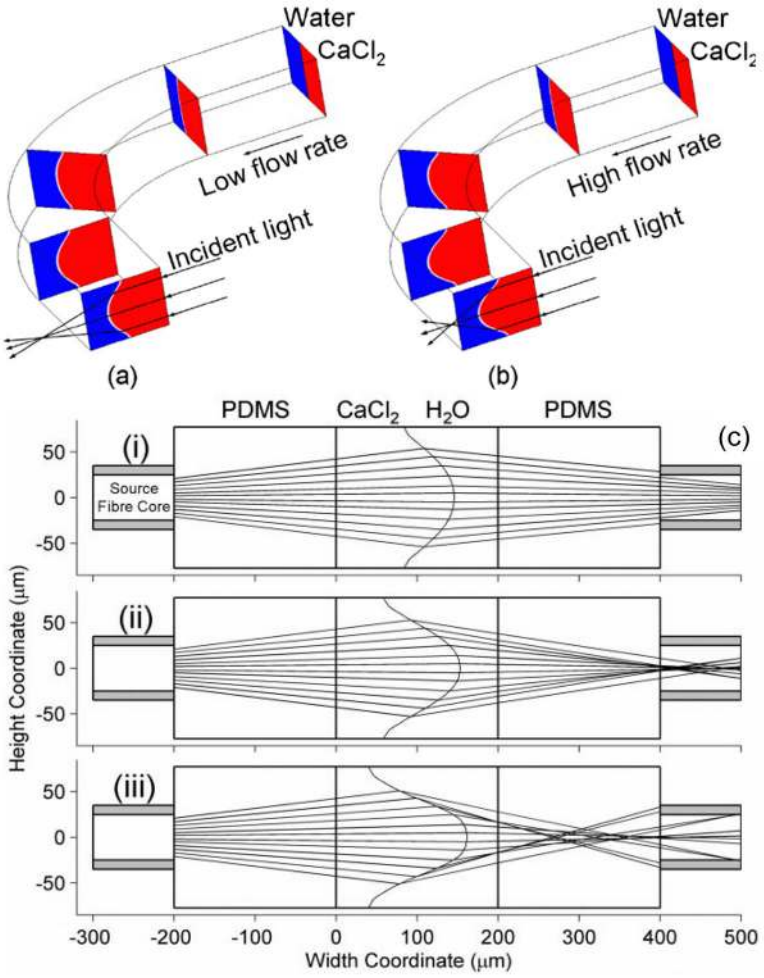

Figure 24.

The mechanism of a hydrodynamically tunable optofluidic cylindrical microlens. $CaCl_2$ solution bows outward into water due to the centrifugal effect induced in the bend of the microchannel. Shorter focal length is obtained after flow transitions from (a) a low flow rate to (b) a high flow rate. (c) Ray-tracing simulation reveals three different focusing patterns: (i) under-focused mode at the flow rate of 150 □ min^{-1}, (ii) focused mode at the flow rate of 250 □ min^{-1}, and (iii) over-focused mode at the flow rate of 350 □ min^{-1}. Reprinted from [111] with permission from *Royal Society of Chemistry*.

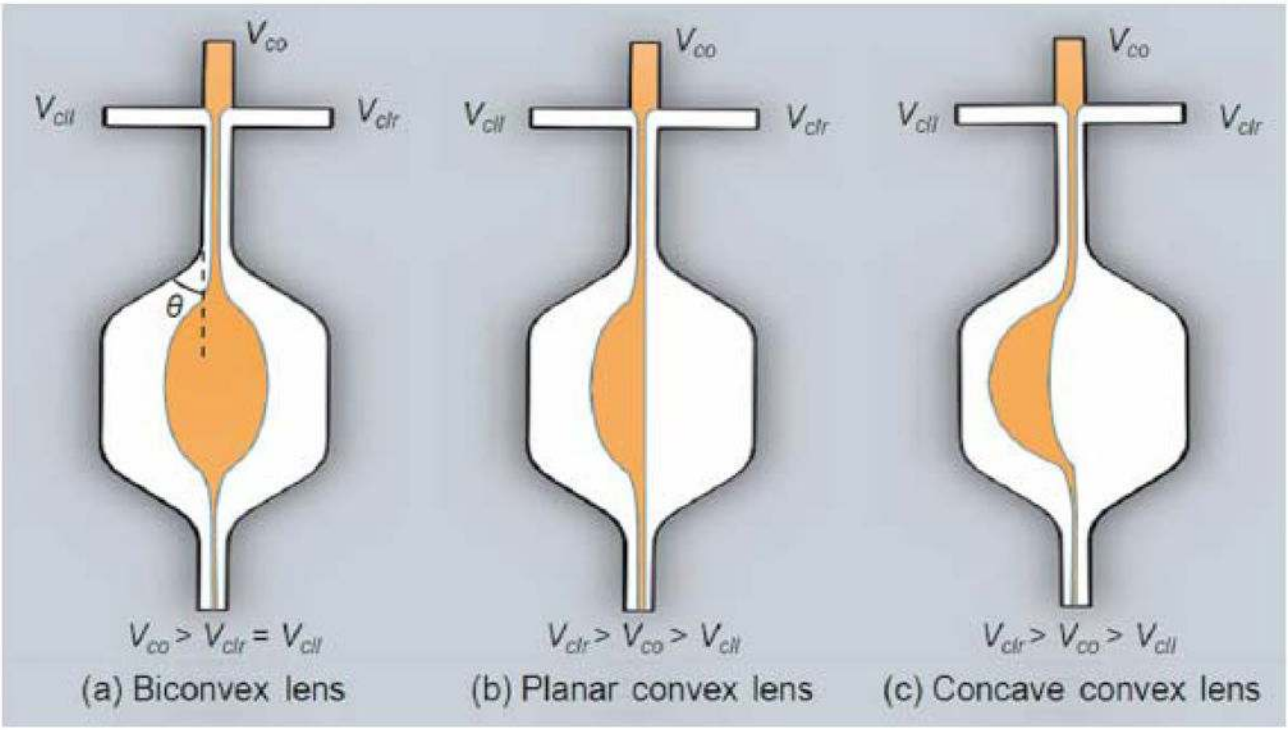

Figure 25.
Schematics of the formation of a tunable liquid microlens dynamically tuned by the flow rates of three streams. Reprinted from [113] with permission from *American Institute of Physics*.

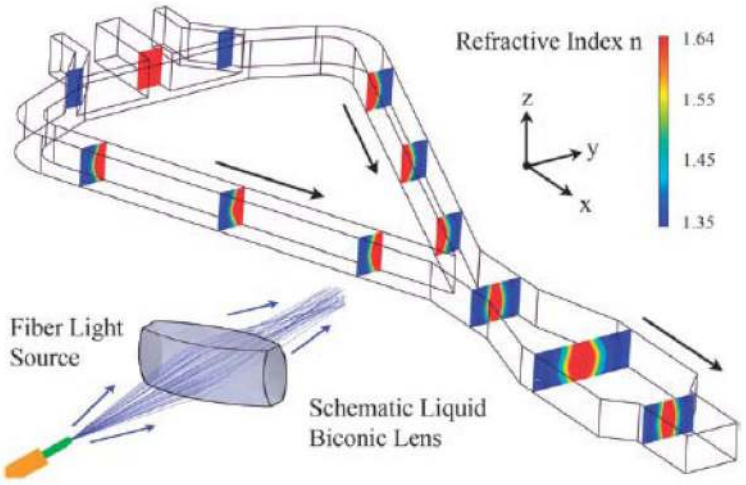

Figure 26.
Schematic of the microfluidic channel design for a 3D optofluidic lens. The displayed cross-sections show the shaping of the lens and the refractive index step defined by the choice of core and cladding fluids. Light path and lens shape are depicted by ray tracing simulation (ZEMAX EE). Reprinted from [114] with permission from *Royal Society of Chemistry*.

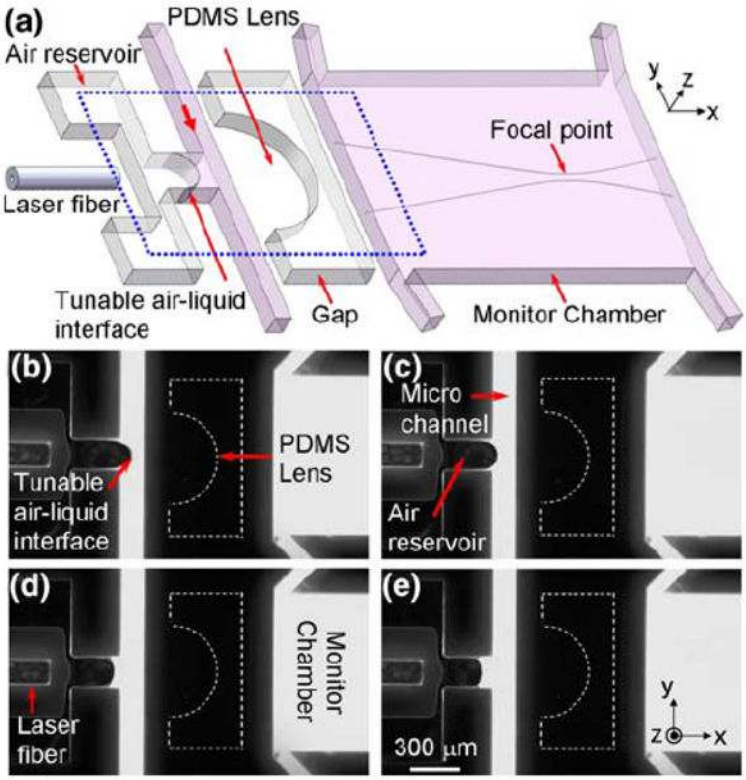

Figure 27.

(a) Schematic of an optofluidic tunable lens. (b) – (e) Optical images of the device (region enclosed by the dotted square in a) taken at different flow rates of DI water in the microchannel Reprinted from [115] with permission from *Springer*.

Table 1

Performance comparison of the existing pneumatically driven polymer microlenses. Reprinted from [61] with permission from *CRC press.*

Author/Reference	Focal length	Pneumatic pressure/Volumetric change	*f*- number	FOV
Zhang *et al.* [52]	8–20 mm	0–15 kPa front lens 0–30 kPa back lens	0.06–0.24	10–80°
Werber and Zappe [53]	1–18 mm	4–54 kPa	n/a	n/a
Chronis *et al.* [19] Jeong *et al.* [54]	0.5–2 mm (oil) 1.8–6.2 mm (Norland 63)	0–35 kPa	n/a	n/a
Chen *et al.* [55]	3.815–10.64 mm	0–70 □L	0.09–0.24	n/a
Feng *et al.* [56]	191–808 mm	0–5 kPa	n/a	10–15°
Agarwal *et al.* [57]	75.9–3.1 mm −75.9–− 3.3 mm	0–14.5 □L 0–13.5 □L	0.61–5.02	0.12–61° double convex 7–69° double concave
Moran *et al.* [58]	2.9–7.5 mm	61–146.9 Pa	0.13–0.35	n/a
Yu *et al.* [59]	10–58 mm	0.2–9.5 kPa	Varied	n/a
Xiong *et al.* [60]	1.9–3.5 mm	11–21 □L	n/a	n/a